POLITECNICO DI TORINO

MASTER's Degree in MECHANICAL ENGINEERING

MASTER's Degree Thesis

Preliminary feasibility study on pyroelectric effect for cooling purposes

Supervisors

Prof. Eliodoro CHIAVAZZO

Prof. Luca BERGAMASCO

Candidate

Giuseppe MARRONE

July 2025

Abstract

The evolution of power electronics world brings a continuous miniaturization of components with an increase in power density. Due to this, thermal management is becoming a critical limit for devices performance and reliability. Traditional cooling technologies go through limitations in efficiency, size, and adaptability, so exploring novel cooling mechanisms is becoming essential to address the increasing heat dissipation challenges in power electronics.

Despite few advancements in conventional and even some emerging applications, the full potential of the pyroelectric effect, a thermally induced polarization phenomenon, for active cooling applications remains largely unexplored. Currently, no known system exploits this effect for convective cooling without the presence of any external electric sources or mechanical parts.

This thesis investigates the feasibility of using the pyroelectric effect, particularly in Lithium Niobate crystals, as a driver for a particular electro-hydrodynamic (EHD) fluid motion, named p-jetting, to create a novel and compact cooling device. The aim is to experimentally verify whether such a system, or in general the p-jetting phenomenon, can outperform natural convection and operate without electrodes or mechanical components.

The study includes a comprehensive literature review of existing electronics cooling methods, followed by theoretical modeling of the pyroelectric effect and its interaction with fluids. A custom experimental setup was developed, including 3D-printed test rigs and precision sensors. Key tests were conducted both at Politecnico di Torino's SMALL Lab and CNR Isasi to evaluate jetting behavior, heat transfer characteristics, and design optimizations under controlled thermal and geometric conditions.

Experimental validation confirmed the generation of fluid jetting due to the pyroelectric effect, especially when using mineral oil as the working fluid. A nozzle-free, electrode-free jetting phenomenon was observed, including a novel against gravity behavior. However, measured heat flux values (4.59 W/m^2) and corresponding heat transfer coefficients (0.17 W/m^2K) resulted significantly lower than those of natural convection.

Even if current results show that pyroelectric-driven fluid motion is feasible and potentially useful for niche applications, the thermal performance is not yet competitive with conventional solutions. Nonetheless, the concept introduces a promising new direction for cooling research, especially in microscale thermal management systems where simplicity and absence of moving parts are critical. This knowledge could potentially be applied in the future to improve the obtained results till satisfying values.

Contents

List of Tables

List of Figures

Acronyms

PE
: Power Electronics

TIM
: Thermal interface materials

EHD
: Electrohydrodynamics

MCHS
: Microchannels

Chapter 1

Electronics Cooling Literature review

As our world moves toward a more industrialized and electrified reality, the need to improve the quality and efficiency of the energy we use and produce is a main issue and an objective of modern research. When approaching the future, the only possibility is an increase in energy demand, even due to the new big challenge we need to face: climate change [1]. The demand for Power electronics to convert and control electrical power will be one of our most important allies in this transition. New technologies and improvements in this field will also lead us to sustainability by reducing the environmental impact by enabling greener and more efficient energy alternatives. [2]. The biggest fields for power electronics applications nowadays are:

- renewable energy systems [3]
- smart grids [4]
- electric mobility [5]

Due to the high power density found in PE systems, efficient thermal management and control is an essential task to accomplish when designing them. Temperature of systems components has a major role in influencing the performance and reliability, so must be always under strict control. Is possible, in fact, to identify for each semiconductor a certain maximum junction temperature, where, surpassing this threshold, can lead to component destruction or permanent damage[6]. Generally these values stay below 85°C in microprocessors with an heat extraction around 100 W/cm^2 and reach till 175°C for modern power electronics transistors like IGBTs, which can even generate heat fluxes in the order of $1KW/cm^2$ in hot spots, and in some cases reach even higher values[7].

Just now, the importance of electronics cooling was clearly highlighted with the direct connection it has to electronics devices failure. The constant progress characterizing the PE world leads to a continuous increase in raw numbers like power, current and, with them, heat generation, due to losses. So, the focus of this chapter will be on the world of cooling and the various technologies that allow future innovations and advancements regarding PE.

At the beginning, a general introduction to cooling theory and basis of thermodynamics will be discussed, after that the topic is switched to the state of the art for electronics cooling methods. Most common solutions are revised, with an historic overview about previous methods and evolution of the state of the art. Finally, a novel method will be introduced with all the advantages it brings and the position it could occupy in the market. All the proposed alternatives will be evaluated with the corresponding data: heat flux $[\frac{W}{cm^2}]$, thermal conductivity $[\frac{W}{m \cdot K}]$, convective heat transfer coefficient $[\frac{W}{m^2 \cdot K}]$.

1.1 Introduction to Heat transfer fundamentals

Cooling can be defined as a particular heat transfer scenario and so to talk about cooling, an explanation regarding the world of thermodynamics is mandatory to understand the topic discussed. The pillars at the base of thermodynamics are the two main laws: *first law of thermodynamics* defines how all the energy that is transferred between systems and inside them can be converted in all the various forms; the variation in internal energy of a system is equal to heat supplied minus work done.

$$dE = \delta q - \delta w \tag{1.1}$$

Instead, *the second law of thermodynamics* expresses the natural movement of energy from an hotter body to a colder one and how doing the opposite is impossible without supplying extra work. This leads to the definition of entropy and to the mathematical formulation of the second principle:

$$dS = \frac{\delta Q}{T} \tag{1.2}$$

Subsequently to these two laws, is possible to split heat transfer between matter into 3 main physical mechanisms: conduction, convection, radiation.

1.1.1 Conduction

Conduction represents the heat transfer happening due to interactions of particles. The particles carrying more energy, when colliding with less energetic particles, transfer a part of their energy. This energy can be defined as random translational

motion or vibrations of particles, that corresponds to what is generally called temperature. So, in presence of a temperature gradient, the heat transfer occurs in the direction of the decreasing gradient. Conduction takes place in all states of matter when a temperature difference is present and the heat flux associated to this principle can be evaluated using Fourier's Law. In one dimensional plane wall[8]:

$$q_x = -k\frac{dT}{dx} \tag{1.3}$$

- q_x - heat flux $[W/m^2]$
- k - thermal conductivity $[W/m \cdot K]$

A minus sign is present due to the gradient of temperature that goes for the decreasing end.

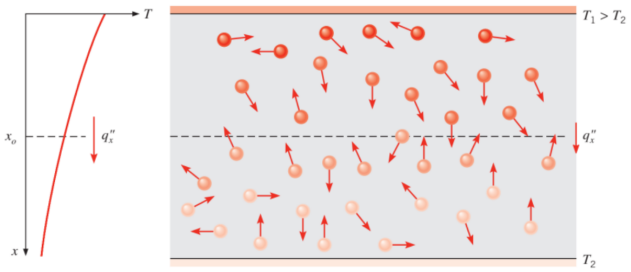

Figure 1.1: Association of conduction heat transfer with diffusion of energy due to molecular activity[8]

1.1.2 Convection

Convection is the second heat transfer mechanism found in thermodynamics and consists of two main principles. In addition to the one already seen in conduction linked to the random movements of particles retaining energy, a second contribution due to the bulk macroscopic motion of the fluid is present. This energy transfer provided by fluid motion is called *advection*. Considering the scenarios in which convection takes place, usually at least one fluid must be involved interacting with a solid surface or another fluid. Since fluid flow is the main reason convection differs from conduction, convection is usually classified by the nature of this fluid flow. *Natural Convection* when the only force that puts the fluid in motion is the buoyancy due to density gradients related to temperature difference. Different is the *Forced Convection* where the movement is caused by an external device or force

such as a fan or a pump. Regardless of the specific case a general equation for convection heat flux can be written in the form [8]:

$$q_{cv} = h \cdot (T_s - T_\infty)$$

- q_{cv} - heat flux $[W/m^2]$
- h - *convection heat transfer coefficient* $[W/(m^2 \cdot K)]$
- T_s - surface temperature [K]
- T_∞ - fluid temperature [K]

TABLE 1.1 Typical values of the convection heat transfer coefficient

Process	h ($W/m^2 \cdot K$)
Free convection	
Gases	2–25
Liquids	50–1000
Forced convection	
Gases	25–250
Liquids	100–20,000
Convection with phase change	
Boiling or condensation	2500–100,000

Figure 1.2: Typical values for convection heat transfer coefficient [8]

1.1.3 Radiation

Radiation is energy emitted by all the matter that has a temperature above 0 degree Kelvin. This energy is transported by electromagnetic waves and does not require any media, so for example, is the main heat transfer mechanism in space. In general, the upper threshold for emitted radiation by a surface is given by the *Stefan–Boltzmann law* which evaluates the max radiation from a *Black Body*.

$$E_b = \sigma T_s^4 \tag{1.4}$$

Due to its nature, radiation is usually negligible for low temperature bodies and takes the lead only in particular scenarios such as vacuum or with transparent bodies.

1.2 Cooling methods state of art classification

As previously discussed, the constant improvement and research in the field of PE brought a wide variety in the cooling methods now known and utilized. The choice of one with respect to another is mostly affected by economic reasons and the application of the particular device. Nowadays, with the increasing power and miniaturization of components, research tends to push dissipation by exploiting novel methods, or to improve the already existing ones to the limits.

However, to have a wider perspective, now a general classification of cooling methods based on the heat transfer media will be discussed, with all the relevant data and appropriate considerations.

1.2.1 Solid-State Cooling

The first medium in contact with the heat source before touching a possible fluid is a solid interface that can be composed of different devices: Heat sinks, Thermal interface materials (TIM), Conduction plates. The heat transmission method for this type of cooling is mainly conduction, so the thermal conductivity of the selected material gets an increasing importance for the choice of the specific device. Here, a review of the three solid-state cooling methods listed above.

- Heat sinks These types of cooling devices are the easiest and cheapest solution for passive conduction heat transfer. The main purpose is to increase the surface area for heat exchange due to natural or forced convection, but to do so in an efficient way the heat sink must be optimized by having the highest thermal conductivity as possible. Due to this characteristic, the natural choices as materials for heat sinks are conductive metals like copper (386 $W/m \cdot K$) and silver (429 $W/m \cdot K$). Since surface exchange area is the main concern in the realization of efficient heat sinks, great attention is focused on the piece geometry: classical solutions include finned surfaces manufactured to interact with the cooling fluid with canals. Heat sinks depending on the application can dissipate till a few W/cm^2 [9].

- Thermal interface materials Connected to heat sinks, TIM represent a solution to the problem of solid-solid surface. In fact, due to low machining accuracy or piece precision, the actual contact area could be a lot smaller than the one of the surfaces in contact (***interfacial thermal resistance***) [10]. TIM are any materials used to fill this gap between the heat source and the heat sink and are designed to achieve the highest heat exchange with the lowest thermal resistance. Most known solutions are *thermal paste*, a polymerizable liquid matrix with a thermally conductive filler and *thermal adhesive*, a type of thermally conductive glue [11].

- Magnetic cooling An alternate cooling solution available for electronics is the magnetic cooling that exploits the magneto-caloric effect (MCE), a phenomenon where magnetic materials change their temperature and entropy when exposed to a magnetic field. This could be compared to the process cooling fluids go through in classic refrigerating cycles. Magneto-caloric effect is most pronounced in magnetically ordered materials, ferromagnets and antiferromagnets, such as *Gadolinium*. Among the advantages of the magnetic cooling we find: low environmental impact, high efficiency and flexibility. The limitations of this solution are linked to: the small temperature range of operation, the low heat fluxes below 1 W/cm^2 and to the problems in having a strong and constant magnetic field due to high costs in magnetic field sources [12].

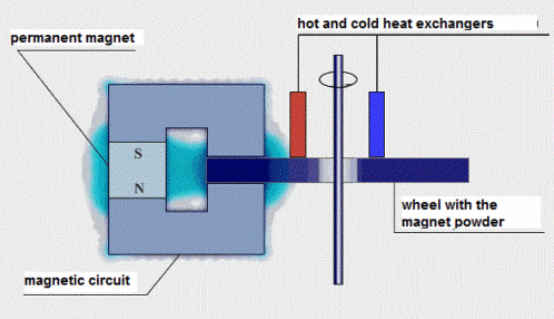

Figure 1.3: Magnetic refrigerator with rotating wheel design containing segments with gadolinium powder [12]

- Thermoelectric cooling This technology relies on the application of a DC current to a number of N-type and P-type thermocouples, generally connected electrically in series and thermally in parallel. The flow of current due to Peltier effect creates a transmission of heat from one side of the cooler to the other, so having one face cooled and the other one heated, in addition, a difference in temperature between the two sides creates a voltage, due to Seebeck effect. Thermoelectric modules generally work with two heat sinks attached to their hot and cold sides in order to enhance heat transfer and system performance.

These types of devices are usually selected for their reliability, absence of moving parts, compact size and no working fluids. However, they cannot be applied extensively due to the high costs and low efficiency, with COP values usually below 0,5 [13]. Values of heat flux for this type of device are generally in the range $1 - 10\,W/cm^2$ [14]

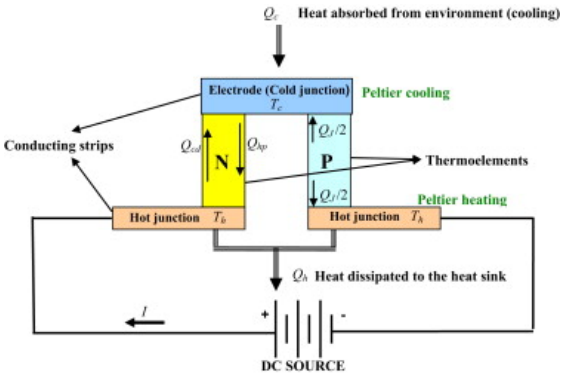

Figure 1.4: Scheme of a thermoelectric refrigerator [13]

1.2.2 Air Cooling

One of the cheapest and simplest choice as cooling fluid is usually air. Air is easily available everywhere and, with its properties, acts as a decent coolant. Air-based cooling methods are mainly based on convection and coupled with optimized heat sinks to increase the surface to fluid contact area. Another relevant parameter when working with air is the fluid velocity, which, depending on the device, can take the lead in the heat exchange efficiency. In fact, most cooling methods in this section will be focused on increasing the value of the convection heat transfer coefficient by creating an air flow.

- Natural air convection This method is used when just a few watts need to be dissipated. Consists in cooling by using still air through convection. The air recirculates due to the buoyancy forces generated by density gradients linked to the temperature increase of the air nearby the heat source. Natural convection cooling is usually coupled with finned heat sinks to increase the surface exchange area. Even with advanced geometries, this cooling method cannot exceed heat flux values of $1\,W/cm^2$ with a coefficient h in the range of 5 to 25 W/m^2K [8].

- Fans: forced air convection Fans are a cheap and simple solution that can provide improved cooling performances with very simple designs and low economic costs. The increase in fluid velocity can highly raise the value of the heat transfer coefficient till values of $250\,W/m^2K$ and consequently improve the heat flux [8]. Although it is a simple solution, fans present some drawbacks related to the low amount of heat they are able to remove, at most a few W/cm^2 for large temperature differences, and the significant noise that large-sized devices can generate when working at max power.

- Piezoelectric cooling This solution is an alternative to traditional fans. Piezoelectric fans work by exploiting the piezoelectric effect to generate an air flow that is easily controllable. The working principle consists in applying an AC voltage to a piezoelectric polymer; due to the voltage, the polymer vibrates with a large amplitude and produces the air movement. These devices show a very high efficiency compared to traditional fans and lower noise, anyway, the very low heat extraction remains a big problem in using them consistently. Piezoelectric fans can hardly double the heat flux values of natural convection, less than $1\,W/cm^2$, and h values that cannot exceed $40\,W/m^2K$ [15] [16].

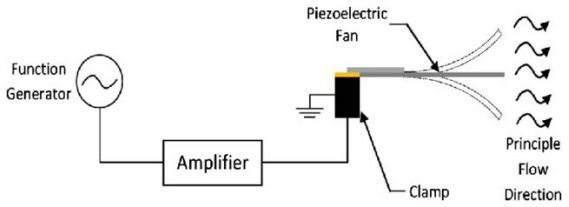

Figure 1.5: Piezoelectric fan scheme [15]

- Synthetic jet impingement Works with the fluid already present in the system, creating these synthetic jets by sucking and ejecting the fluid from an orifice. The movement is induced by the vibration of a diaphragm, so the concept is very similar to the piezoelectric fans. Due to the vibrating motion, the jet impingement has a certain controllable frequency that shows a greater heat absorption with respect to a single continuous jet. In addition, this control of the volume of working fluid sprayed onto the heated surface allows the user, in a much shorter time, to control the temperature of the heated surface and thereby the heat transfer. These jets can be single or multiple and reach values of heat transfer coefficient h even ten times greater than natural convection, around $150\,W/m^2K$, with heat fluxes around $2-3\,W/cm^2$ [17] [18].

- Electrohydrodynamics (EHD) Electrohydrodynamic (EHD) flow is a phenomenon that occurs when a corona discharge is generated in a gas at atmospheric pressure, forming a type of non-thermal plasma. This electrically induced airflow is commonly referred to as ionic wind or corona wind. On a macroscopic level, ionic wind represents the direct transformation of electrical energy into the kinetic energy of a moving fluid. On a microscopic scale, it results from momentum being transferred from free electrons and charged ions. Thanks to its unique physical properties, EHD technology offers several benefits, including fast response time, low energy consumption, silent operation, and the ability to produce airflow without any moving mechanical parts. These characteristics make EHD systems very suitable

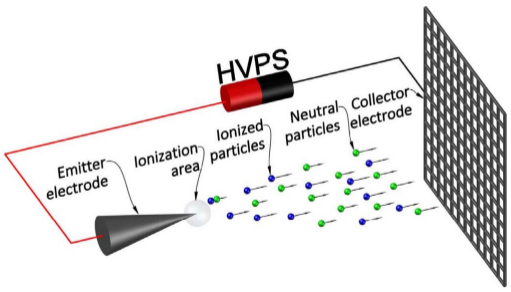

Figure 1.6: Particle stream of a dc EHD device [19]

for forced convection heat transfer, where ionic wind generators are used to improve cooling efficiency. Numerous studies have focused on refining electrode designs and optimizing configurations to maximize the thermal performance of these systems. In certain configurations, the convective coefficient of micro fabricated ionic wind pumps reached values of $3200\,W/m^2K$ with a heat flux removal up to tens of Watts [20]. The downsides of this technology are represented by the limited cooling power with respect to liquid cooling, the degradation of electrodes, and the safety concerns regarding the high voltages [19].

- Thermo-acoustic cooling This innovative cooling method works with sound waves as heat engines to pump heat from a cold environment to a hot environment. A thermo-acoustic device does not have any moving parts and simply consists in using sound waves in an inert mixture of nonflammable gas like helium, argon, or air. In general, two categories for this type of device are defined: either 'standing-wave' or 'traveling-wave'. This technology is very promising for the future due to its eco-friendly nature and as an alternative to traditional heat-driven cooling. Unfortunately, low values of COP and efficiency represent a big obstacle in the diffusion of this cooling method and for the moment the values of heat flux cooling remain barely higher than natural convection [21].

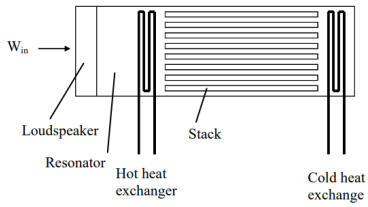

Figure 1.7: Standing wave Thermo-acoustic engine [21]

1.2.3 Liquid Cooling

Liquid cooling represents the preferred solution in electronic cooling due to clear advantages in heating removal performance of water, or liquids in general, with respect to air. Firstly, water thermal conductivity is 0,58 $W/m \cdot K$ in comparison to the air one that is 0,024 $W/m \cdot K$ at 20°, so quite 20 times more. In addition, the same can be said for the specific heat capacity, that for water is 4184 $J/Kg \cdot K$ while the air value is 993 $J/Kg \cdot K$ at 20°. These values bring an increase in cooling density and so a reduction in size of water cooled devices with constant or improved cooling performances with respect to air driven ones. Even the convective coefficient for water goes up to thousands of $W/m^2 \cdot K$ in forced convection with respect to the max 350 $W/m^2 \cdot K$ obtainable with air. Disadvantages of liquid cooling are: possible corrosion, leaks, electrical problems, higher cost, maintenance, etc. [8].

Liquid cooling can be divided into direct or indirect contact: direct contact if the fluid touches or submerges the electronic device, indirect contact if it is separated from the heat source by a conductive wall or heat sink. Now a list of liquid cooling solutions is presented, with both technologies.

- Cold plates An indirect liquid cooling device that works by recirculating a fluid in various channels that cool down a plate in direct contact with the heat source. The fluid is recirculated by a pump and needs an heat exchanger to dissipate the excess heat. With particular channels and plate geometries the heat transfer coefficient values can reach up to 30.000 W/m^2K with heat fluxes even above 100 W/cm^2 [22].

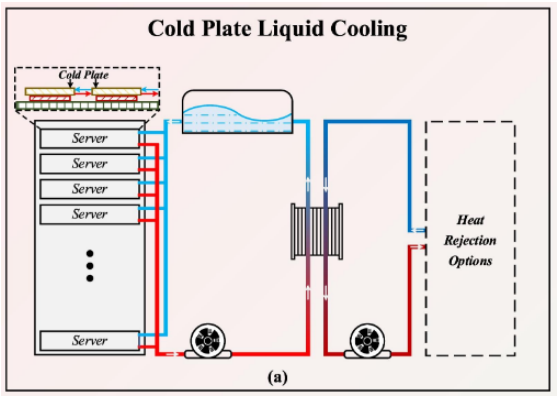

Figure 1.8: Cold plate cooling scheme for data center [23]

- Single-Phase Microchannel An improvement with respect to cold plates is represented by microchannel cooling, due to the enhancement in heat transfer while maintaining similar characteristics. The biggest advantage is the great increase in surface-area-to-volume ratio, that enables the device to remove large amounts of heat even from small areas. Even with their limitations, high pressure losses and severe risk of clogging due to the small section of the channels, the performance of this technology are remarkable if compared to the fact that it is an indirect cooling method and is relatively simple. Researchers have studied various ways to overcome the limitations of this method: more powerful pumps and sectioning the circuit in shorter lengths to reduce the pressure losses, or a filtering system to solve the clogging problematic. Regarding the fluid, the best choice is usually water due to the excellent thermal properties; however in some cases water retains problems: first, the proximity to high voltage devices, brings risk of a discharge event, another problem is that the freezing requirements for electronics applications (-40 °C) are much lower than the freezing point of water. While there are alternatives to water, such as dielectrics and antifreeze mixtures, their use not only results in higher heat sink thermal resistances, but it also exacerbates pressure losses due to increased viscosity. Lastly, another possibility is using stacked micro-channels to further decrease the thermal resistance and the pressure losses for each layer added [24]. Here below, a table with thermal values for single phase MCHS 1.1.

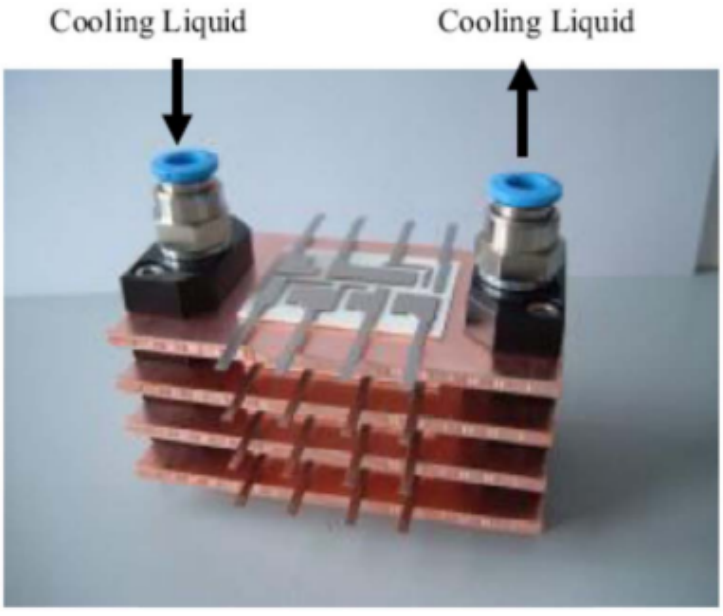

Figure 1.9: Stacked microchannel [24]

Table 1.1: Single-phase MCHS data [24]

Ref	Mat	Fluid	$T_d - T_i$ (C)	q" (W/cm^2)	h_{eff} (W/cm^2K)	COP
[28]	Si	water	63	300	3.57	359.5
		water	63	304	3.62	354.6
[29]	Cu	water	100	604	1.96	33.1
[31]	Cu	water	15.4	-	1.05	634.1
[40]		CuO–water	23	42.6	1.85	23255.8
[41]	Si	water	67.5	417	4.63	378.2
[42]	Si	water	47	170	3.61	3472.2
[43]	Cu	water	20	73.6	2.39	547.4
[44]		EGW	75	100	1.25	459.8

*Mat = MCHS material, EGW = 50/50Ethylene-glycol/water

- Electrowetting A particular direct cooling system that implies the use of liquid droplets controlled with an electric field. These devices can work efficiently because the droplets can be redirected to the most critical spots of the electronic device, like the hot spots, that can reach very high temperatures over 150°, and dissipate the excess heat with direct convection. Relevant parameters are: the velocity of the droplets, the flux rate of droplets in a second, the dimension of the droplets. The transport and manipulation can be controlled by programmed electrical signals to reach high levels of customization and adaptation to the particular case [25]. In addition, to reach higher dissipation values, instead of cooling by exploiting sensible heat transfer, phase change heat transfer can be chosen; evaporation or boiling of the droplets. In general, well-designed devices can reach up to 40-50 W/cm^2 of dissipation with h coefficient around 10.000 W/m^2K [26].

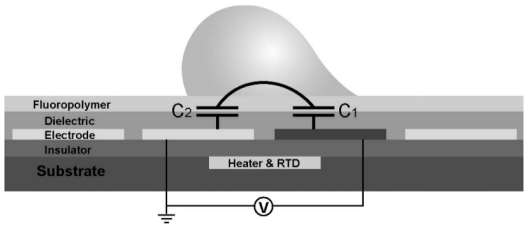

Figure 1.10: Cross-sectional view of Electrowetting-induced liquid droplet actuation [25].

- Immersion cooling The immersion cooling technique represents an advanced thermal management approach that employs a dielectric liquid to dissipate heat through convection, subsequently releasing it into the environment via either single-phase or two-phase mechanisms. This method offers several key advantages, including, a high heat transfer coefficient, stable hydrodynamic behavior, and the ability to directly cool heat-generating components through liquid contact. Commonly used dielectric fluids include mineral oil (MO) and virgin coconut oil (VCO), both of which are widely recognized for their thermal performances. Immersion cooling is typically applied in various electronic systems such as computer servers, data centers, photovoltaic (PV) modules, battery packs, and power transformers. A notable benefit of immersion cooling is its capability to cool the entire surface area of components, in contrast to indirect cooling methods, thereby improving thermal uniformity and reducing localized heating on both positive and negative electrodes. High efficiency can be achieved by selecting a coolant with high thermal conductivity, low viscosity, and a high heat capacity. A single-phase immersion cooling is usually a recirculating cooling system without any phase-phenomena; the heat is transferred through direct convection with the electronic heat source, cooled through a heat exchanger in the coolant distribution unit (CDU), and then discharged to the ambient by a cooling tower. However, some challenges associated

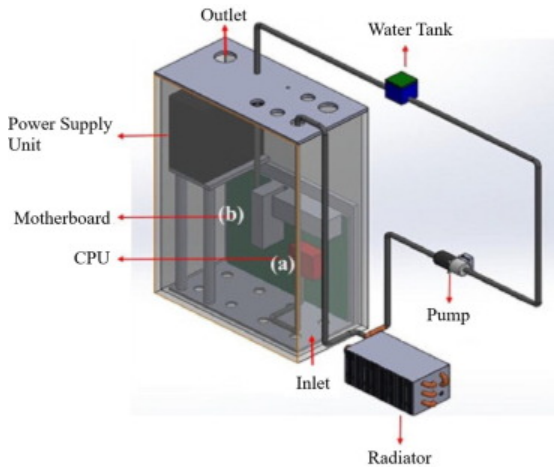

Figure 1.11: Single-Phase cooling typical circuit [27].

with this technique include the risks of electrical short circuits and electrochemical corrosion [28]. Generally, single-phase immersion cooling devices show heat fluxes around 500 W/cm^2, but in particular forced convection cases can reach up to 1000 W/cm^2 [27].

- Jet-impingement Jet impingement cooling technique consists in high momentum fluid jets that strike the heat source substrate, granting a pretty high heat-transfer and the possibility to keep operating the device. In addition, due the possibility to easily localize the cooling, this technology is very well suited for hot spot heat removal. The jets of cooling liquid come from an array of nozzles powered by a pump system that creates the required pressure gradient to overcome the fluid shear. This configuration, with very thin thermal and velocity boundary layers, keeps the system really efficient with a very high heat transfer coefficient Fig 1.12. Jets can be classified based on the fluid kinematic as: laminar, transitional, or

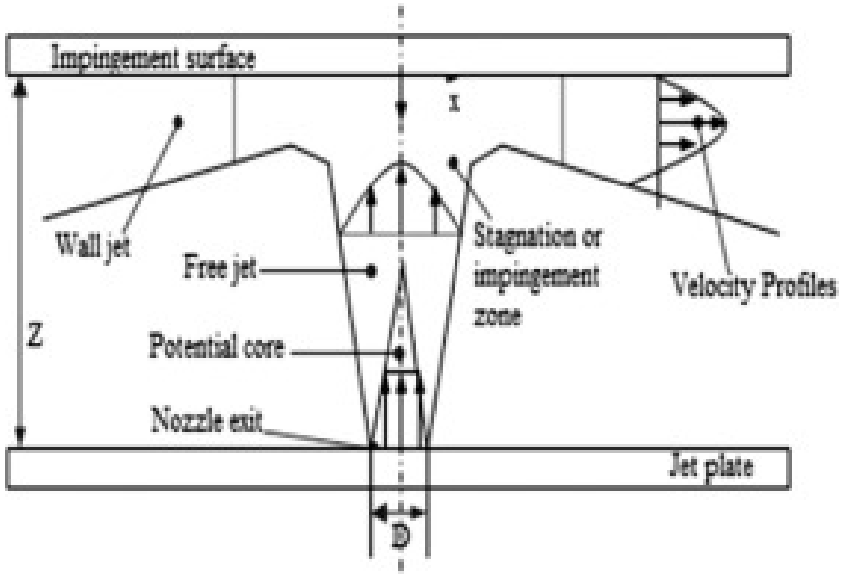

Figure 1.12: Orthogonal jet impingement on a heated substrate [29].

turbulent. This classification is strictly linked to *Reynolds number*, jet diameter, and average fluid velocity. The best performance are obtained with turbulent jets, that, with their high transport rates, can reach higher values of heat removal. To achieve more efficient configurations, the best solution is to use a multiple jet array. Jet impingement cooling is usually chosen due to the high thermal performance (one of the techniques with highest heat flux, around 1000 W/cm^2, but has been recorded even 2000 W/cm^2 [29]) and very small drawbacks, like the pressure losses that are still lower than micro-channels in the same conditions. Even values of heat transfer coefficient can reach record values, as stated in Natarajan and Bezama [30], with recorded values of coefficient h above 100000 W/m^2K.

1.2.4 Two-Phase Cooling

To support the need for always higher cooling density devices, the latest innovation in this field is represented by two-phase cooling technology. As the name explains, these devices exploit the phase change of the working fluid to increase the heat removal by adding to the sensible heat, the latent vaporization heat capacity of the fluid. Due to this improvement, same values of heat flux can be dissipated with a smaller device-fluid exchange area, or with reduced flow rates. Clearly, the addition of another heat transfer mechanism brings a whole lot of problems in simulations and, predicting the behavior of the fluid is not trivial; however this is the target of the research that continuously tries to overcome these challenges.

- Heat pipes Heat pipes, which operate based on the phase change of a working fluid within a sealed structure, represent a highly effective method for cooling electronic devices such as computers, laptops, telecommunications systems, and satellite modules. Owing to their exceptionally high effective thermal conductivity, extremely greater than that of copper (400 W/mK), and their very low effective thermal resistance, typically in the range of 0.05 to 0.4°C/W, heat pipes are among the most efficient solutions for dissipating the high heat flux generated by components such as central processing units (CPUs) [31]. A heat pipe is composed of a metallic enclosure (typically a cylindrical pipe), a wick structure, and a working fluid. It is generally divided into three sections: the evaporator, the adiabatic section, and the condenser. The wick, usually attached to the inner wall of the pipe, plays a critical role in the operation of the heat pipe. It enables capillary pumping, which transports the condensed fluid from the condenser back to the evaporator, even against gravity. This mechanism allows the heat pipe to function effectively in any orientation. In the Fig **1.13** we can look at a schematic of an heat pipe. The working principle consists in the creation of a pressure difference due to phase change in the evaporator, the pressure drives the vapor to the condenser to cool in the heat sink, and then in liquid state goes back to the evaporator through the wick porosity. Heat pipes cooling is suitable for various applications due to their high heat transfer capacity, fast thermal response, reliability, and compactness; in addition, is characterized by the absence of moving mechanical parts. Such properties make this cooling method suitable for both long and short time spans with maximum values of h coefficient around 10^5 W/m^2K and heat fluxes even above 100 W/cm^2 [32].

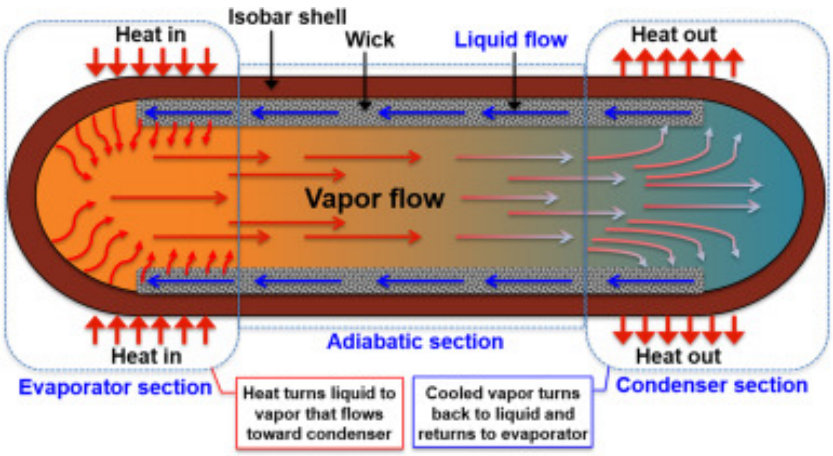

Figure 1.13: Schematic of a heat pipe [31]

- Two-phase Microchannel With respect to the single phase solution in this case there are two main benefits: enhanced heat removal rates and improved temperature uniformity along the cooled surface. This because the boiling provides the additional component of latent heat removal and as a plus, since the boiling is an isothermal process, the temperature uniformity obviously benefits from this. As a result temperature gradients along the flow path as low as 0,7 $\circ$C/mm for a heat flux of 255 W/cm^2 have been reported [24]; a value that is three times smaller than with comparable single-phase cooling. Different liquids can be implemented in this device to enhance the thermal performance, an example is represented by Lee and Mudawar [33] that tested the R134a in a micro-channel heat sink incorporated as an evaporator in a refrigeration cycle. The results showed values of convective coefficient as high as 50.000 $W/m^2 \cdot K$ and heat fluxes around 100 W/cm^2 [33].

- Spray cooling Another technique that relies on phase change to enhance heat exchange is spray cooling. Regarded as one of the most efficient cooling methods for electronics, due to the extremely high heat flux removal for tiny surfaces with small temperature rises. Spray cooling stands out for its combination of uniform surface temperature distribution, low coolant flow requirements, and low surface superheat. Spray cooling involves converting the cooling fluid into fine droplets of a specific size using a nozzle. These droplets continuously strike the heated surface, creating a thin liquid film that enhances cooling through mechanisms such as forced convection and boiling.

Among the most important choices to obtain an optimal spray cooling: nozzle type, flow rate, spray distance, coolant used, etc. Regarding the best coolant, an interesting choice could be water, due to the optimal heat removal properties; however, maximum importance is given to the boiling point. which for water is

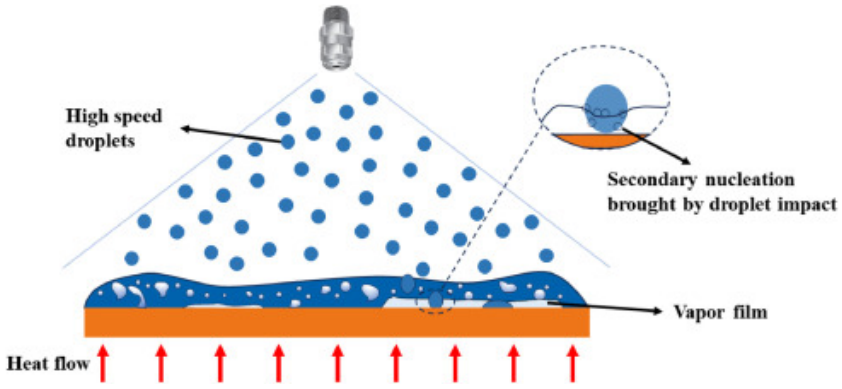

Figure 1.14: Schematic of spray cooling on heated surface [34].

too high to operate in a lot of fields. In the literature, a wide variety of liquids has been used as coolants: Pais et al. [35] reached a record 1200 W/cm^2 by using an air-water atomizing nozzle, LIU et al. [34] achieved a maximum CHF of 341 W/cm^2 with liquefied natural gas (LNG), Bostanci et al. [36] succeeded in using ammonia with values of heat flux around 500 W/cm^2. As can be seen from results the heat flux attest around 500 W/cm^2 with values of convective coefficient h even above 50.000 $W/m^2 \cdot K$ [34].

These results encourage research in spray cooling technology that seems very promising for the future of high-power electronics, even with all the difficulties that arise from the study's complexity of this method.

- Two-phase Immersion cooling Two-phase immersion pool boiling represents the direct advancement of its single-phase counterpart. The cooling is performed, at the same time, through natural convection, forced convection, and boiling; this grants the method remarkable heat removal values, plus very high temperature uniformity. Bubbles formation creates a natural movement of the water that recirculates without the use of any pump or similar devices. To complete the circuit, the vapor is then cooled and condensed via some kind of air-cooled heat sink already inside the tank.

As for the single-phase alternative, the preferable liquid choice would be a dielectric to avoid any electric interaction problem with heated devices, but due to the higher thermal properties, even deionized water could be chosen using appropriate electrical insulation. In addition, the phase-change adds the constraint of high boiling temperature of the liquid, which represents an upper threshold that cannot be surpassed.

This technology has been demonstrated by Birbarah et al. [37] to achieve higher heat fluxes in water till 562 W/cm^2 with respect to dielectric fluids 111 W/cm^2 with h coefficients in water till 50.000 $W/m^2 \cdot K$. Kibushi et al. [38] showed

that particular heat sink geometry - lotus copper - paired with a particular effect called "breathing phenomenon" the heat flux values can raise till 534 W/cm^2 with a convective coefficient as high as 126.000 $W/m^2 \cdot K$ always using water. They even reported other configurations in previous papers with values greater than 800 W/cm^2, under sub-cooled pool conditions using micro-bubble emission boiling [38].

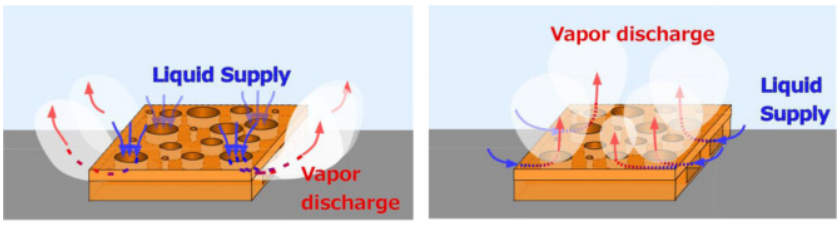

(a) Mode G (b) Mode L

Figure 1.15: Breathing phenomenon schematic [38].

1.3 State of art final review

As depicted in the previous description of the various cooling methods, our era is characterized by an exceptional variety of solutions for cooling that space in every range of values from a few W/cm^2 till thousands. Same can be said for the values of heat transfer coefficient with an even bigger numerical gap; here a summary table of the technologies previously analyzed with respective numerical values Fig 1.16.

The table speaks itself: optimal technologies for big amounts of heat dissipation are liquid and two-phase cooling solutions. Naturally, with higher heat fluxes comes an increase in complexity and in costs. Liquid cooling technologies, for example, show big issues with pressure losses and mostly need an additional forced convection recirculation system to work. Even two-phase technologies, seem very promising for the future, but at the moment the complex nature of the physics involved is an enormous challenge to overcome.

In general what can be said, is that each cooling method must be chosen for the particular application, keeping in mind the pros and cons of every possibility. Heat flux value is obviously a fundamental parameter, but to reach the optimal, attention must be put even on efficiencies, reliability, hot spot removal, costs, packaging density, flexibility, easy access and replacements exc... In fact, all the technologies seen before have their spot on the market, as an example, when simplicity and low cost are the priorities, with a small thermal load, air cooling solutions represent

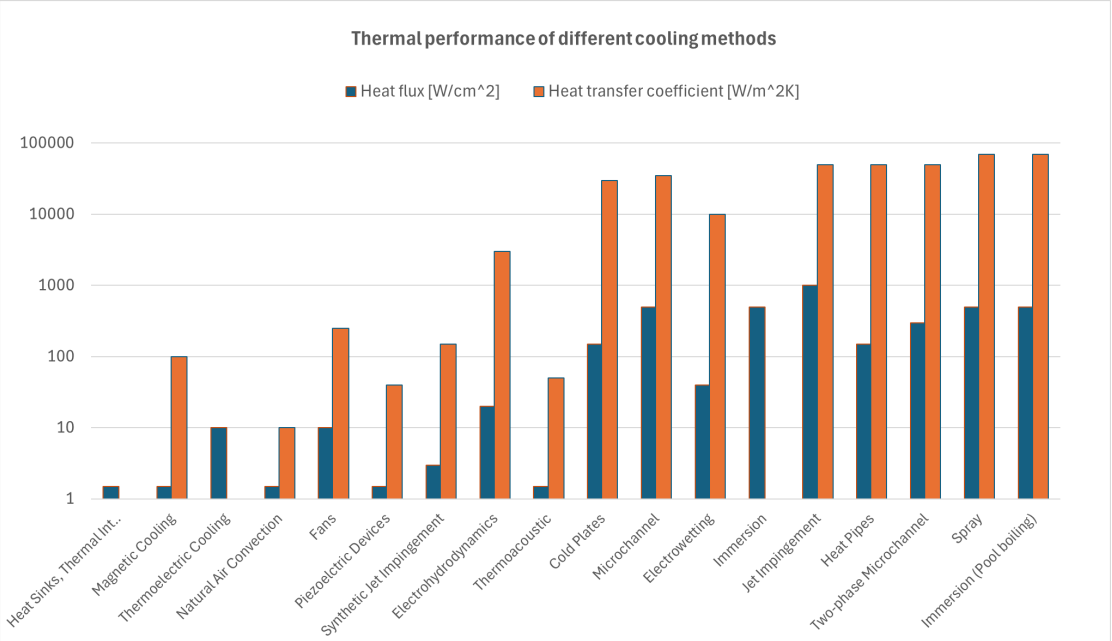

Figure 1.16: Graphical review of cooling techniques

the best choice. All this shows how much important research in all fields is for, reducing energy waste and optimizing Power Electronics cooling.

Chapter 2

Fundamentals and Applications of the Pyroelectric Effect

Since the main topic of this thesis is to introduce the possibility of applying the pyroelectric effect in the world of electronics cooling, in the current chapter a comprehensive description of the so-called effect will be presented, to better understand what will come next.

2.1 Description of the effect and LiNbO3 crystal properties

Pyroelectricity is a particular effect usually manifested in piezoelectric materials that consists in the polarization change of a material when its temperature is changed from an equilibrium value. The polarization brings an accumulation of charges on the two surfaces of the material with a specific directional gradient. Due to this separation, an electric field is manifested by the crystal that is proportional to the temperature gradient.

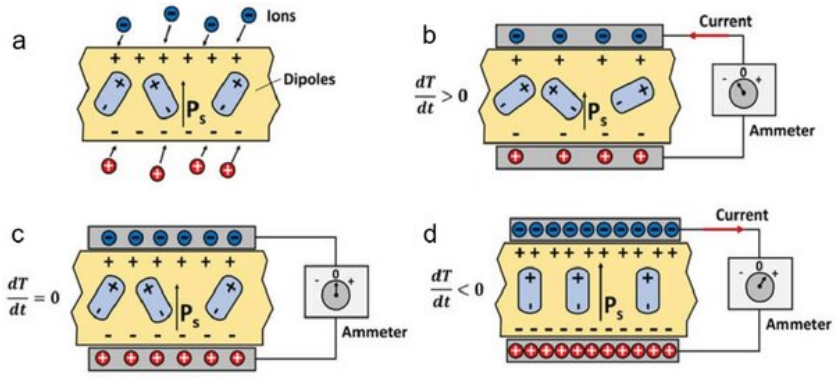

Figure 2.1: Working mechanism schematic based on the pyroelectric effect.
a) Spontaneous polarization in pyroelectric materials arises from internal electric dipoles.
b) When $\frac{dT}{dt} > 0$, the spontaneous polarization decreases, prompting electron flow through the external circuit.
c) When $\frac{dT}{dt} = 0$, the internal electric field from spontaneous polarization is balanced by the induced external electric field at the electrodes, maintaining equilibrium.
d) When $\frac{dT}{dt} < 0$, the spontaneous polarization increases, disrupting the electrical balance and causing electrons to migrate in the opposite direction [39].

Documented first by the ancient Greeks around 600 BCE, pyroelectricity has been used since 1960 mainly for detector and sensor applications [40]. Pyroelectric materials can convert even small thermal fluctuations into electricity, so they can be used for harvesting thermal energy from ambient with efficiencies higher than those of *TEGs* with *Seebeck effect* or for certain high-precision thermal sensors.

A multitude of pyroelectric materials exists, that span from mineral crystals, mainly tourmaline (alumina-borosilicate with various impurities), while synthetic pyroelectrics are lithium sulfate (LiSO4 × H2O), lithium Niobate (LiNbO3), potassium tartaric acid (K4C8O12 × H2O), and many others. The focus of the thesis will be mainly directed to the *Lithium Niobate*, since this crystal will be implemented for the testing throughout the whole experimental procedure.

2.1.1 Pyroelectric coefficient and performance indicators

The pyroelectric coefficient represents the ability of a material to respond to temperature-induced changes in polarization intensity. In pyroelectric materials, variations in temperature cause a change in the polarization, which is reflected in the dielectric displacement (D) of the material, defined as:

$$D = Q/S = \epsilon E + P \tag{2.1}$$

- Q - pyroelectric charge [C]

- S - surface area of electrode $[m^2]$
- ϵ - dielectric constant
- E - external electrical field [V/m]
- P - polarization $[C/m^2]$

For a constant stress and electric field, pyroelectric coefficient can be rewritten:

$$p = (dP/dT)_{\sigma,E} \quad [C/m^2K] \tag{2.2}$$

- σ, E - constant conditions

If the temperature is considered constant along the surface with an invariant pyroelectric coefficient, the pyroelectric electric current (i_p) is defined:

$$i_p = dQ/dt = pS(dT/dt) \tag{2.3}$$

- dT/dt - rate of temperature change in time

Once the polarization or density of charge (P) is defined, this value is found inside the formula for the potential difference on the crystal surface:

$$\Delta U = \frac{P \cdot d}{\epsilon_0 \cdot \epsilon_r} \tag{2.4}$$

- ΔU - Potential between the two faces of the crystal [V]
- d - thickness of the crystal [mm]
- ϵ_r - relative dielectric constant of the crystal

- FOM Due to the diversity of applications for pyroelectric materials, and the variety of materials belonging to this category, three main *figure of merits* (FOM) had been defined in the literature to classify the performance of this class of materials:

$$FOM_i = p/c = p/(\rho c_p) \tag{2.5}$$

- ρ - density of pyroelectric material $[Kg/m^3]$
- c_p - specific heat of pyroelectric material $[J/Kg \cdot K]$

Equation 2.5 refers to the current-sensitive readout.

$$FOM_y = p/(\rho c_p \epsilon_0 \epsilon_r) \tag{2.6}$$

- ϵ_0 - vacuum dielectric constant
- ϵ_r - relative dielectric constant of pyroelectric material

Equation 2.6 evaluates the voltage response. Lastly, for pyroelectric detectors:

$$FOM_D = \frac{p}{\rho c_p \sqrt{\epsilon_0 \epsilon_r tan\delta}} \tag{2.7}$$

- $tan\delta$ - dielectric loss

Above equation 2.7 is used to evaluate the detection capability [39].

2.1.2 Insight on pyroelectric materials

In recent times, pyroelectric materials have seen an increasing diffusion in all research fields. The variety of applications is strictly linked with the requirement of different properties depending on what is needed for each specific case. As an answer, great attention is given to pyroelectric materials design with different structures and consequently properties. Pyroelectric materials can mainly be classified in 4 classes: single crystals, ceramics, inorganic films, and polymers and composites.

- Single crystals Single crystals are widely researched in the pyroelectric field due to their excellent stability and controllability through regulation of crystal structure, orientation, and doping. *Triglycine sulfate* (TGS) is a well-known single crystal studied since the 1960s, typically grown via cooling or solution evaporation. Its pyroelectric performance is affected by orientation and temperature. Thin films containing TGS nanocrystals show a temperature-dependent pyroelectric coefficient that first increases and then decreases in the range from 25 to 50 °C. Crystal orientation also plays a key role in the pyroelectric behavior of Mn-doped $94.6Na_{0.5}Bi_{0.5}TiO_3$-$5.4BaTiO_3$, with the orientation exhibiting the best performance due to alignment with the direction of spontaneous polarization. The pyroelectric coefficient increases from 6×10^{-4} to 7×10^{-4} $C{\cdot}m^{-2}{\cdot}K^{-1}$. The thesis study material, the $LiNbO_3$, belongs to this class of pyroelectric materials.

- Ceramics Ceramic materials are widely used in pyroelectric, piezoelectric, and ferroelectric applications due to their easy preparation, low cost, good mechanical properties, and tunable electrical characteristics. Pyroelectric performance can be enhanced through doping, phase optimization, and synthesis improvements. A key category is perovskite ceramics with the general formula ABX_3, where A is typically a rare earth or alkaline earth metal, B is a transition metal, and X is an oxide or halide. Notable perovskites include $BaTiO_3$, $BiFeO_3$, and $Pb(Zr, Ti)O_3$.

- Inorganic films Inorganic pyroelectric films have gained significant attention due to their low thermal capacity, cost-effective fabrication, and flexibility, making them ideal for wearable electronics. These films are typically fabricated using mature techniques such as:

- Sol-gel method
- Magnetron sputtering
- Chemical vapor deposition (CVD)
- Atomic layer deposition (ALD)

Multilayer composite films like BFO/PZT(30/70) and BFO/PZT(70/30), fabricated via sol-gel and spin coating, show distinct pyroelectric behavior. The BFO/PZT(30/70) film exhibits temperature-independent performance, whereas the BFO/PZT(70/30) shows higher sensitivity to temperature variations.

- Polymer and Composites Polymers and their composites are widely used in everyday life due to their nonconductivity, light weight, flexibility, low cost, and ease of mass production. With advances in polymer technology, functional polymers such as pyroelectric polymers and composites have been developed and applied in thermal energy harvesting, temperature sensing, and wearable electronics. Among these, polyvinylidene fluoride (PVDF) and its composites are the most studied pyroelectric materials.

2.1.3 LiNbO3 crystal

The crystal adopted for the thesis pyroelectric effect induction is Lithium Niobate (LiNbO3). Lithium Niobate is a ferroelectric crystal that belongs to the trigonal crystal system, is transparent between 0.25 and 5.3 μm and can be used in visible, near IR and middle IR region. As any ferroelectric, Lithium Niobate demonstrates piezoelectric effect, nonlinear optic effects, photo-elastic effect and Pockels effect (linear electro-optic effect). What makes Lithium Niobate stand out is that the coefficients characterizing these effects are several times greater than those of similar ferroelectrics, facilitating its usage for various applications.

Physical properties of lithium Niobate crystals are summarized in the table below:

Table 2.1: Key physical properties of optical grade non-doped lithium Niobate crystals [41].

Property	**Value**
Crystal structure	Rhombohedral, space group R3c, point group 3m
Primitive cell dimensions (Å)	a = 5.148, c = 13.868
Refractive indices	$n_o = 2.220$, $n_e = 2.146$ @ 1300 nm $n_o = 2.232$, $n_e = 2.156$ @ 1064 nm $n_o = 2.286$, $n_e = 2.203$ @ 632.8 nm
Optical homogeneity (cm^{-1})	$\sim 5 \times 10^{-5}$
Density (g/cm^3)	4.64
Curie temperature (°C)	1157
Melting point (°C)	1253
Mohs hardness	5
Thermal expansion coefficients (@25°C, K^{-1})	$\parallel c = 4 \times 10^{-6}$, $\perp c = 15.7 \times 10^{-6}$
Thermal conductivity ($W/(m \cdot K)$)	$\parallel c = 4.61$, $\perp c = 4.19$
Specific heat capacity ($J/(kg \cdot K)$)	648
Shear modulus (G) (Pa)	7.99×10^{10}
Elastic constants (GPa @298 K)	$C_{11}^E = 204$, $C_{33}^E = 246$, $C_{44}^E = 60$, $C_{13}^E = 75$, $C_{14}^E = 9$
Piezoelectric constants (C/N)	$D_{22} = 20.8 \times 10^{-12}$, $D_{33} = 6.5 \times 10^{-12}$
Dielectric constants (@300 K)	$\varepsilon_{11}^T/\varepsilon_0 = 85.2$, $\varepsilon_{33}^T/\varepsilon_0 = 30$ $\varepsilon_{11}^S/\varepsilon_0 = 45$, $\varepsilon_{33}^S/\varepsilon_0 = 27.5$
Nonlinear optic coefficients (m/V)	$d_{33} = 37.8 \times 10^{-12}$, $d_{31} = 5.1 \times 10^{-12}$, $d_{22} = 2.46 \times 10^{-12}$
Sellmeier equation coefficients (λ in μm)	$n_o^2 = 4.9048 + \frac{0.11768}{\lambda^2 - 0.04750} - 0.027169\lambda^2$ $n_e^2 = 4.5820 + \frac{0.099169}{\lambda^2 - 0.04443} - 0.02195\lambda^2$
Damage threshold (MW/cm^2, 10 ns @1064 nm)	100
Water solubility	Insoluble
Pyroelectric coefficient	p = -8,3 $\cdot 10^{-5}\, C \cdot m^{-2} \cdot K^{-1}$

2.2 Patents and devices featuring Pyroelectric effect

In this chapter, few applications of the pyroelectric effect from scientific papers will be discussed and analyzed. The studies are conducted by the CNR Isasi in Pozzuoli and mainly cover the usage of Pyroelectricity for their laboratory purposes: micro-optical and biological research.

2.2.1 Accumulation of Tiny Aqueous Droplets Using a PyroElectric Jet System

First article published on AEM journal in 2021 by V. Tkachenko et al. covers the possibility of using Lithium Niobate crystals to generate high electric fields, on the order of kV/mm, to accumulate tiny aqueous droplets for bio-molecules detection purposes. [42].

These fields were used for ejecting tiny daughter droplets from the free meniscus of a mother drop with a sub-μl volume. This is called PyroElectroHydroDynamic jet or p-jet with the big advantage that it is nozzle-free and electrode-free, thus allowing to avoid the typical clogging drawbacks encountered in conventional pipetting systems and ink-jet printers. The p-jet is obtained by applying an appropriate heating ramp through a Peltier element on a small piece of LiNbO3 crystal, thus achieving good control of the jetting operation. A quasi-static pyroelectric field is generated that slowly decays due to the attraction of charges from the environment to the crystal surface. This technology has been found useful for accumulating protein-based or sugar-based molecules by printing several droplets in a restricted area through the p-jetting. Here, a scheme of the discussed setup:

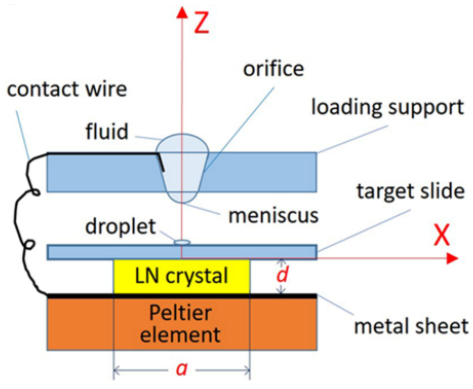

Figure 2.2: Schematic of the micro-droplet p-jet configuration [43]

2.2.2 Pyro-electric solar energy harvesting device based on LiNbO3 crystals

In 2014 Luigi Battista et al. published an article on Applied Energy journal about a novel scheme for solar energy harvesting based on pyroelectric effect [43].

The idea is based on an optical system focusing solar radiation on a Lithium Niobate crystal. Solar radiation heats up the crystal inducing a thermal gradient, that produces a charge accumulation on the crystal due to pyroelectric effect. However, direct solar exposition of pyroelectric harvester does not always allow to reach enough wide amplitude of the temperature variation. The innovation is coating one face with a nano-composite material that greatly increases the absorption, inducing a wider thermal gradient on the crystal and improving the overall efficiency of the device. Mainly, two different carbon-based black radiation absorbent coatings have been used on the z-face LiNbO3 crystals: carbon black (CB-carbon nanopowder graphitized, <200 nm size, >99.95%) and graphene (reduced graphene oxide).

The charge produced will be then stored in a capacitor, and the electrical power that flows can be found as:

$$P_{CE} = \frac{dE_{CE}}{dt} = \frac{d}{dt}(\frac{1}{2}C_E \cdot V_{CE}^2) = C_E \cdot V_{CE}(t) \cdot \frac{dV_{CE}}{dt} \tag{2.8}$$

Below a scheme with the main features listed before in the paper and experimental setups:

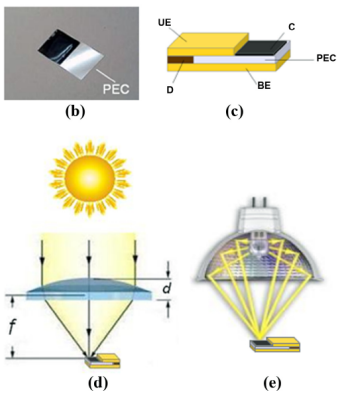

Figure 2.3: Scheme of solar energy harvesting device features [42]:
(b) Pyro-electric element with absorbing coating.
(c) Scheme of pyro-electric sample attached to metal electrodes.
(d) Scheme of optical focusing system used outdoor
(e) Scheme of experimental setup used in laboratory.

Chapter 3

Flux sensor Analysis and Validation procedure

3.1 Working principle literature review

The main component of the workbench thought for the cooling device testing is the flux sensor. The flux sensor used includes a very particular working principle, that exploits simple concepts to work efficiently. The sensor is introduced and described in depth by Eliodoro Chiavazzo et al.2014 [44]. The device in Fig 3.1, 3.2 utilizes a copper sample upon which the convective heat transfer coefficient is to be measured and exploits the notion of thermal guard.

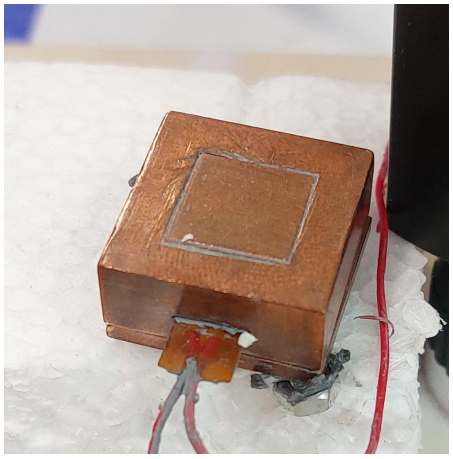

Figure 3.1: Flux sensor photo

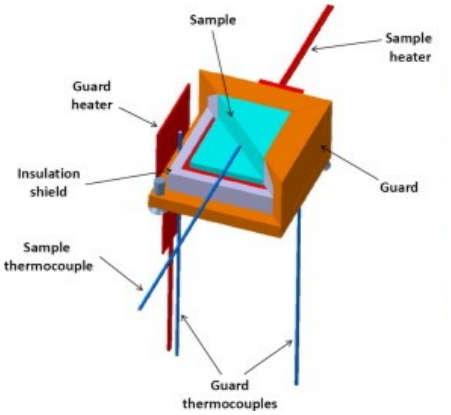

Figure 3.2: Flux sensor working scheme [44]

The guard has the ability to prevent undesired heat flows and can be conveniently used for measuring convective heat transfer coefficients. Sensors exploiting this concept can be so accurate that are sometimes used even for calibration purposes.

The sensor is made of three parts: the sample, the insulation shield, and the guard. The sensor presents an onion-like structure: the insulation shield wraps the sample, while a highly conductive guard wraps the assembly consisting of both the sample and the insulation shield Fig 3.2. In addition, two heaters are placed, one heats the sample and the other heats the thermal guard. With this configuration, two thermal circuits are obtained: sample heater generates the thermal power to be removed by the tested surface, while guard heater supplies thermal energy to the guard until an isothermal condition is reached.

The heaters used were commercial polyimide mat heaters of 10 mm x 10 mm surface. The insulation shield is made of Teflon and thermal grease was used for reducing thermal resistances at all contact surfaces of the device, when appropriate. Sample and guard are made of copper and both present practical 0,5 mm diameter holes to insert thermocouples for temperature measurements. Three type K thermocouples with probe sheath diameter of 0.5 mm are used. One reaches the center of the sensor sample, while the other two are inserted symmetrically in the guard. This enables to check that only a minimal temperature difference is established between two sufficiently far locations of the guard. Second, imposing the sample temperature equal to the arithmetic mean of the two temperature values in the guard, grants a minimal net heat exchange between sample and guard.

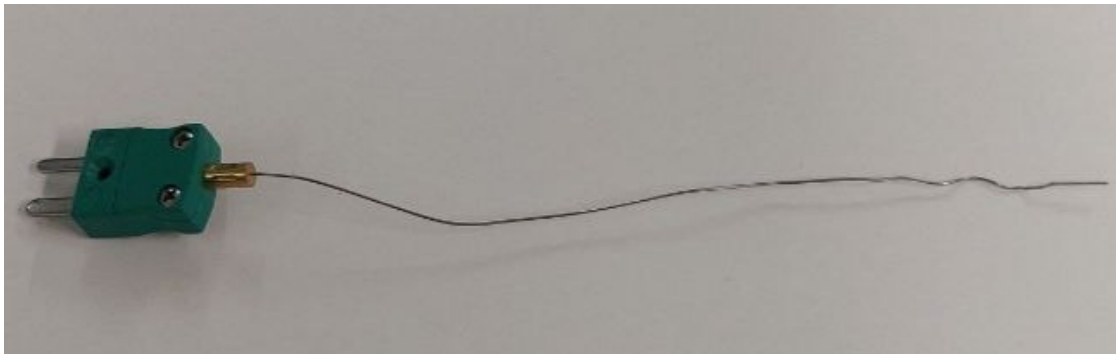

Figure 3.3: Thermocouple used for testing

The working principle of the sensor consists in evaluating the heat flux coming out only from the top face of the sample that has a known dimension of 1 cm^2 to have a clear estimate of the heat flux. When the heaters are turned on, the goal is to heat up both parts of the sensor with adjustable powers until the isothermal condition is measured by the thermocouples. Once so is done, since the sample is surrounded by the guard at the same temperature, the heat coming from the internal heater is forced to be dissipated all through the top face of the sample, the only face exposed to air, that is of our interest. The interaction between sample

and guard is regulated by the Fourier law:

$$q_x = -k\frac{dT}{dx} \tag{3.1}$$

As can be seen when the dT is absent the heat transfer is null. The value of power supplied to the sample is the exact measure of the heat flux through the top face of the sensor. If the surface is known an accurate measure of the heat flux can be carried out by simply dividing the electrical power for the surface net of losses.

3.2 Testing strategy and validation

Two tests were conducted to verify the reliability of the sensor: natural convection and forced convection with a fan. The objective was to verify that the convective coefficient h values, evaluated through the sensor, were consistent with the literature. To perform the measurements, the power supply was providing two separate voltages, one to the sample heater and one to the guard heater, for each test. Here in Tab 3.1 a summary of the results obtained for both cases.

Test	**Natural c.**	**Natural c.**	**Forced c.**	**Forced c.**
Power Supply	P.S.1 (Sample)	P.S.2 (Guard)	P.S.1 (Sample)	P.S.2 (Guard)
Voltage [V]	1.3	6.7	3.3	7
Current [A]	0.07	0.22	0.122	0.25
Power [W]	0.091	1.474	0.405	1.75
Steady state T [°C]	76		49.4	
h [W/m^{2}K]	16.25		137.83	
Ambient Temp. [°C]	20		20	

Table 3.1: Test values and results for flux sensor validation.

The value of the h coefficient was obtained from the convective heat equation:

$$W = h \cdot A \cdot (T_{sens} - T_{amb}) \tag{3.2}$$

- W - power supplied by the heater to the sample equal in value to the heat dissipated [W]
- h - convection coefficient needed to compare the sensor measurements with literature values $[W/m^2 \cdot K]$
- A - heat exchange surface, in this case equal to 1 cm^2 $[cm^2]$
- T_{sens} - temperature at which the steady state is reached in the sensor [°C]
- T_{amb} - ambient temperature [°C]

Temperatures data were acquired through a data acquisition device specifically designed for thermocouples from National Instruments. The device connected to the laptop via USB, and the data were processed using a measuring software called LabVIEW. LabVIEW registered the temperature values in real time from thermocouples inserted in the flux sensor.

The charts below show the temperature trends obtained for our testing workbench Fig 3.4, 3.5. In the lower figure, it is possible to notice the reaching of the steady state temperature with a superposition of the three curves with minimal temperature difference (in this case less than 0,5 °C). That portion of the graph is of our interest for the recorded values seen in the table above.

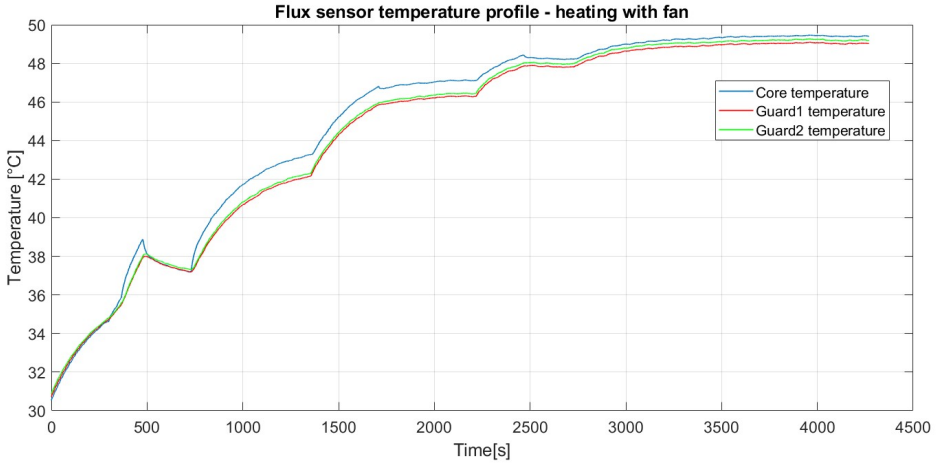

Figure 3.4: Flux sensor heating till steady state with fan

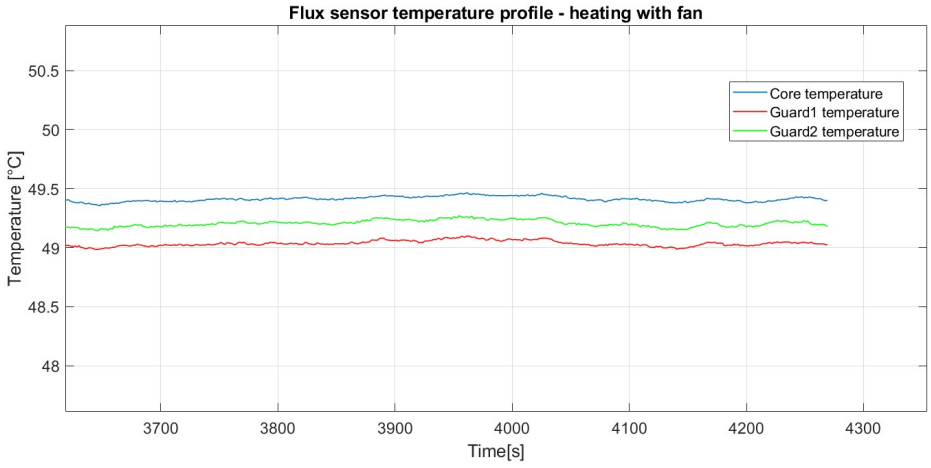

Figure 3.5: Steady state temperature zoomed section

Through comparison with literature values:

Condition	**Heat Transfer Coefficient h ($\mathbf{W/m^2 \cdot K}$)**
Air — natural convection	2–25
Air — forced convection (low speed)	10–100
Air — forced convection (high speed)	100–250

Table 3.2: Heat transfer coefficient h for air under different convection regimes (literature values).

The h estimations in Tab 3.1 are comparable with the actual values, so the sensor can be considered reliable for testing. If high precision is needed, the temperatures from both the sample and the guard must be the same; the more they get close, the more the measurement obtained from the sensor will be precise.

Chapter 4

Pyroelectric effect induction Testing

Here the main chapter of the thesis begins, a description and resume of the way all the results obtained were achieved. The methodology includes all the test setups used to record data and actually produce the effect, plus an overview of all the software and techniques employed. Through this section a step by step depiction of the thesis work will be shown with all the passages followed in temporal order from the beginning.

The experimental work mostly takes place at the Polito SMALL lab inside the DENERG department, under the direction of Professor Chiavazzo and Bergamasco. However, a brief portion of testing occurred at the ISASI CNR of Pozzuoli (NA) thanks to researchers Sara Coppola and Pietro Ferraro. One of the following sections will provide a detailed account of the activities carried out there. Now the thesis will focus on the main concept: pyroelectricity exploitation for electronics cooling purposes. This design is completely novel and consists in taking advantage of the temperature induced electric field to have an Electro hydro-dynamics based convection cooling.

4.1 Cooling device concept

The first design suggested by Professor Chiavazzo, can be seen in Fig 4.1.

From this figure, a general overview of the working principle can be understood by looking at the various picture components:

- **The CPU heat source**: represents the device that needs to be cooled hypothetically, it could be a CPU or electronic component that undergoes some kind of self or induced heating.

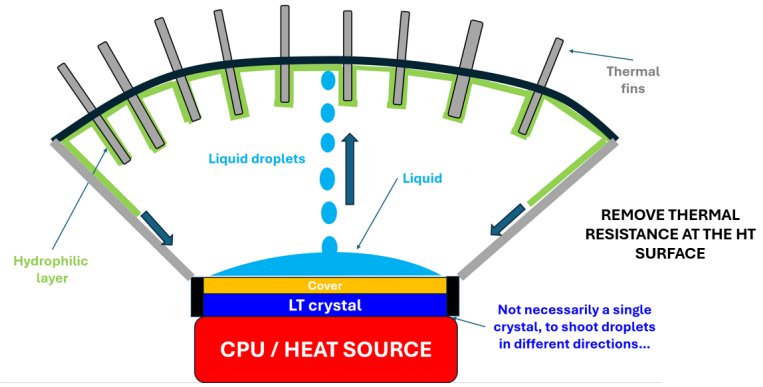

Figure 4.1: First pyroelectric cooling device concept

- **LT crystal**: is the main component, the pyroelectric crystal in the study case a $LiNbO_3$ crystal, the optimal dimension and geometry will be discussed later.
- **Cover**: a conductive material layer used to have separation between the crystal and the working fluid while allowing heat exchange.
- **Liquid reservoir**: the working liquid pool that has the role of transferring heat through forced convection.
- **Finned heat exchanger**: just a temporary design for the coupled heat exchanger to cool the liquid before it returns to the hot pool.

The design simplicity is one of his strong points, now a brief depiction of the general functioning of the device will be presented:

- Pyroelectric crystal heating The contact between the crystal and the heat source will produce a ΔT on the $LiNbO_3$ this will induce an electric field due to charge accumulation on the faces of the crystal. So, the self-inducted electric field will then act on the pool of heat transfer liquid, generating an EHD liquid motion towards the heat exchanger. This motion, coupled with the upper cooling from the heat exchanger, will grant a passive cooling of the upper crystal face.

- Liquid EHD motion The main physical phenomenon that produces the convective motion needed to achieve a cooling heat flux is the EHD jetting. The jetting is obtained when the electrostatic force resulting from the normal component of the electric field is sufficient to overcome the surface tension of the working

fluid. A stationary droplet, in Fig 4.2 positioned on a capillary nozzle, will not flow until a force is applied which will overcome the surface tension and capillary forces by which it is held. When an electric potential is applied to the system, charge will migrate to the meniscus surface of the liquid and when sufficient charge has built up on the fluid interface, an electrostatic potential is created between the meniscus and the grounded substrate. At a certain point, normal stresses destabilize the meniscus, and the tangential component supports the formation of the meniscus into a cone (termed a Taylor cone) which results in jetting. Since

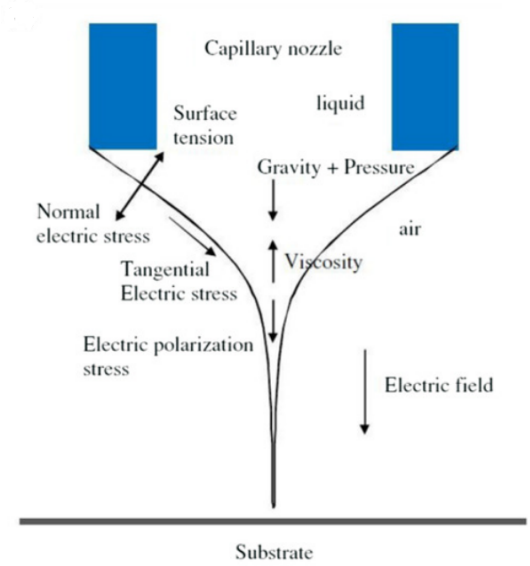

Figure 4.2: Summary of forces acting at capillary tip during EHD jetting [45]

in this thesis work the electric potential exploited to produce the EHD jetting is supplied by a pyroelectric crystal, the particular phenomenon studied will be called EHD p-jetting from now on.

- Heat exchanger design and consideration The top part of the device has significant relevance since it is responsible for both the cooling and the recirculation of the liquid after the jetting phenomena. A first concept as seen in Fig 4.1 includes some air-cooled, possibly detachable, fins to ensure the right amount of heat transfer and a porous material on the base of the heat exchanger. The porous material is needed to ensure that the liquid and the fin stay enough time in contact to transfer all the heat and to guide the liquid back to the hot reservoir above the crystal.

The objective of the device is to reach heat transfer values at least higher than those shown by natural convection. The biggest advantages of this technology, that would represent a big improvement to classical EDH, is the total absence

of electrodes to generate the electric field and of any moving mechanical part. Other than this, usually to have an EDH jetting, a nozzle is required to give the appropriate shape to the liquid pool. In this case, the device is nozzle-free and so is free from clogging problems of any type. In addition, the manufacturing costs would be low enough, as the device is fairly small and the materials involved are easily available. So, thanks to its simplicity, the finished device could represent a nice innovation in the field of PE cooling and the goal of this thesis is studying the possibility to introduce it at least as a concept.

4.2 Prototyping with 3D printer

The SMALL lab has inside two functional 3D printers: an Ultimaker 3 and a Stratasys Elite. 3D printing is the most efficient solution to craft an optimal testing setup without any time losses due to shipping or missing pieces problems. First goal was prototyping in SolidWorks a dimensionally accurate testing workbench for the flux sensor discussed in chapter 3. The initial design and dimension came from the proposed device sketch seen before, while including as the heat source instead of a real CPU the copper flux sensor.

Both printers had been used, but the Stratasys, thanks to the higher dimensional accuracy and printing velocity, was selected for printing the various pieces. Before starting the printing process, a preliminary material analysis was conducted to select which ones were suitable for the print: decent heat resistance, good mechanical strength, high dimensional accuracy exc..

Materials	**Tensile Strength [MPa]**	**Thermal Resistance [°C]**	**Hardness Shore D**	**Impact Strength [kJ/m²]**
PLA	53 - 59	59	84	4
ABS	34 - 40	87	76	14
NYLON	63 - 65	89	81	14
CPE	42 - 50	77	76	6
CPE+	40 - 48	100	77	37
PC	65 - 72	111	81	12
TPU 95A	20 - 27	116	48	36
PP	10 - 12	99	42	49
PVA	/	/	/	/

Table 4.1: 3D printer filaments properties

Finally the material chosen for the printing was the ABS, due to the high thermal resistance and decent tensile strength with good resilience. Below a picture

of the product label found on the material box:

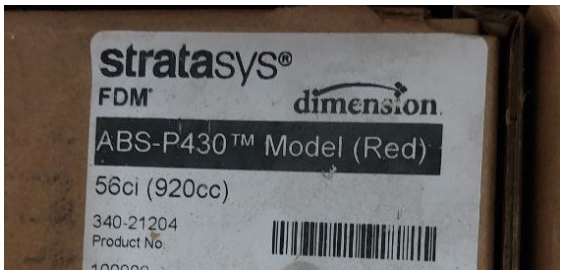

Figure 4.3: Product label for ABS 3D printer material

The testing setup design started from the inferior part; this because the upper part with the heat exchanger would have needed a proper in-depth study, and since it was not the main priority, the design was postponed. The main goal of the geometries was to accommodate the heat source/flux sensor in a designated space while granting access to all the temperature sensors, in this case K type thermocouples with 0,5 mm diameter. In addition, the upper part of the printed pieces Fig 4.6 had a geometry that led to the formation of the liquid pool seen in the preliminary design.

After gaining confidence with the 3D printer the geometries were finalized with all the right dimension and the possibility to be assembled both with and without screws granting quick and simple disassemble when needed or good resistance with screws on. Here some pictures of printed design:

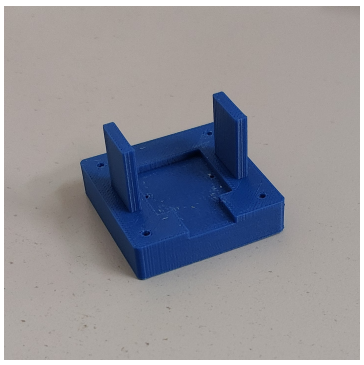

Figure 4.4: Lower piece

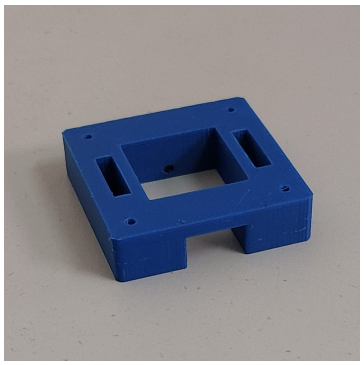

Figure 4.5: Middle piece

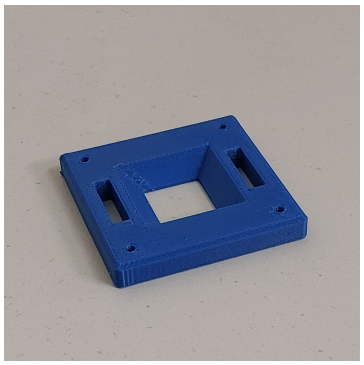

Figure 4.6: Upper piece

Except for these preliminary prints, the usage of the 3D printer will be a constant during the whole thesis testing process. Later on, all the pieces manufactured with the printer will be depicted with figures and brief descriptions.

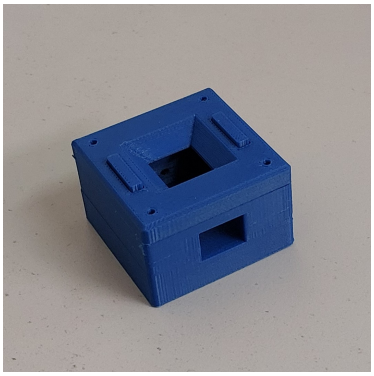

Figure 4.7: Fully assembled geometry

4.3 First tests performed on pyroelectric crystal

The crystal was sent at SMALL lab from CNR Isasi of Naples, where they laser cut the crystal for the thesis testing purposes. As seen before, the crystal is a Lithium Niobate cut with precise dimensions requested for experimentation: a 10 mm x 10 mm square base surface with a thickness of 2,5 mm Fig 4.8. The surface is almost the same of the flux sensor and is pretty convenient for heat flux measurements since it is already 1 cm^2. As seen in chapter 2, there is a linear relationship between thickness and generated potential, so it was demonstrated that a 2,5 mm thickness was enough to obtain decent values of electrical voltage. Moreover, a differentiation must be made between the two faces of the crystal called Z- and Z+. The face Z- is marked with a superficial cut noticeable in Fig 4.8 and demonstrated to be the best one for obtaining the effect.

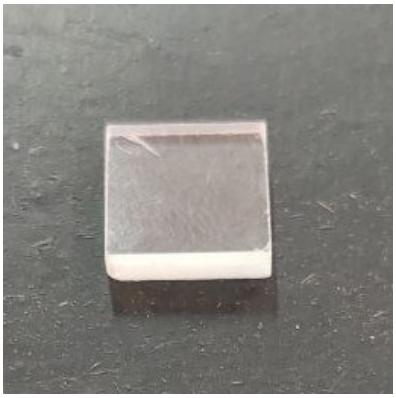

Figure 4.8: LiNbO3 crystal used for testing

At first, LiNbO3 was tested with the printed geometries seen before, the flux sensor with heaters was below, and on the top surface the pyroelectric crystal was put to heat up and generate the electric field. The printed geometries were adapted to host the crystal and to sustain above it a liquid pool to observe the effects of the electric field. The liquid employed was distilled water to avoid any clogging issues. However, these initial tests gave no visible results: liquid remained still in the reservoir without any movement, while the crystal, heated by the flux sensor, experienced various temperature cycles.

After several failed attempts, the approach was changed: the objective was to gain a clear idea of the testing condition to trigger the pyroelectric effect and to obtain a first view of the effect to better understand it and evaluate its magnitude. To accomplish this, the 3D printed geometry was put aside to utilize a new setup made of:

1. Magnetic heating plate as heat source
2. Standard pipette to put the liquid on top of the crystal
3. Heat sink to cool the crystal
4. New set of testing liquids sent from CNR Isasi

Liquids sent from Naples included:

- Mineral oil m3516 from Sigma-Aldrich
- Glycerol to make solutions with water at various percentages
- Various cooling fluids, namely, Cool 2 cutting fluid form Buehler

The tests were performed by pouring a variable amount of liquid with the pipette directly over the crystal and moving it with pliers over the hot plate. Plate temperature oscillated from around 80 - 100 °C, while the heat sink quickly cooled the crystal back to ambient temperature around 20 °C. In this case, throughout the testing, some kind of effect was visible. The liquid during the crystal heating tended to experience some bubbling, while moving to the sides of the Niobate surface. Everything stopped when the temperature gradient for the crystal ended after a few seconds, while more bubbling occurred in the cooling phase.

These results were not sufficient to understand the effect and not comparable to the liquid jetting that was expected. Movements confirm the presence of an electric field generating from the crystal, but the magnitude is not enough to form

a Taylor cone and a subsequent liquid jet. In addition, from this test the liquid that showed the greatest impact was the mineral oil, instead the other liquids hardly experienced any effect.

The high difficulty in comprehending the optimal setup to actuate the desired p-jetting, brought as a solution a brief visit to the CNR Isasi laboratory. They were able not only to obtain the effect, but to use it for innovative research purposes as the ones seen in section 2.2, so entering their lab was the fastest way to understand and master the pyroelectric effect.

4.4 CNR Isasi testing

During a 2 week period, various tests were conducted at CNR Isasi to learn about the conditions to obtain the pyroelectric effect and to ensure reproducibility for future experiments. Now, a brief introduction to the workplace. The Institute of Applied Sciences and Intelligent Systems "Eduardo Caianiello" (ISASI) conducts research in the fields of Physics, Information Science, Neuroscience, and Biology. The research carried out at the Institute is characterized by a high degree of thematic specialization, while also offering the potential to address multidisciplinary challenges. ISASI is part of the Department of Physical Sciences and Matter Technologies (DSFTM) of the National Research Council of Italy (CNR). The research areas include: study of imaging, microscopy, and optical analysis; photonics and optoelectronics; functional devices, sensors, and biosystems; information science and artificial intelligence. The thesis project was conducted with the help of researchers Sara Coppola, Pietro Ferraro and part of the staff. They gave access to laboratories and instrumentation, while explaining the p-jetting reproducibility condition, following the thesis project step by step.

4.4.1 Mounted test setup with Peltier

First test had the objective of having a clear view of the effect in a proven environment with accurate video data acquisition and well known experimental variables. This test setup was already installed and utilized for experimental purposes in other pyroelectric applications such as the ink-jet printing previously seen in subsection 2.2.1.

The mentioned testing workbench included:

- **A Peltier cell**: works as a heat source for crystal heating, can work both in heating and cooling. Such kind of cooling device falls in the category of thermoelectric cooling 1.2.1
- **A LiNbO3 crystal**: 10 mm x 10 mm square base with 2,5 mm thickness, needed to obtain a consistent effect.

- **A microscope slide**: the liquid droplet is positioned on the microscope slide facing the crystal at the bottom with a certain measured distance between the two.

- **A PDMS hydrophobic substrate**: needed to keep the droplet in place, hanging against gravity from the glass slide, while granting an high contact angle to the liquid.

- **A precision monochromatic micro-camera**: really important to acquire video data and observe the effect in a clearer way.

Here, a schematic of the discussed setup with all the various components clearly recognizable.

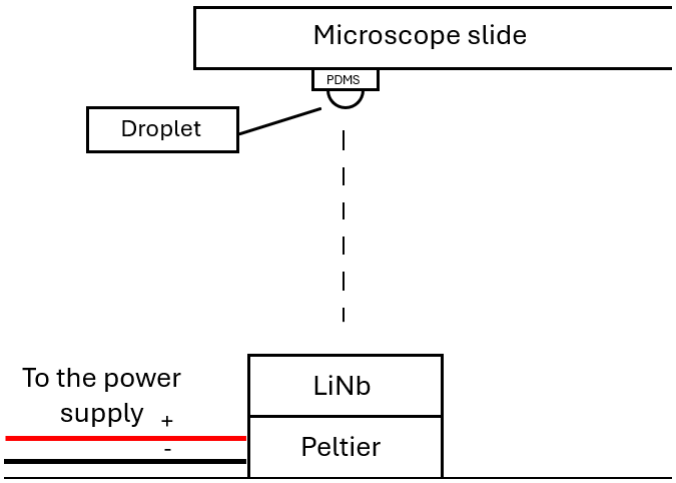

Figure 4.9: Schematic of Peltier setup at CNR Isasi with various components

For the liquids, CNR Isasi provided various samples, majority of them already tested in Turin. Below Tab 4.2 with all the liquids and mixtures used in the tests with respective properties.

Test were performed always with the same iterative procedure: a liquid droplet was positioned on the PDMS substrate on the glass slide. The slide was put above the crystal at a known distance and the Peltier was turned on heating the pyroelectric until the visible effect on the liquid was exhausted, due to the absence of a temperature control.

Liquid	**Viscosity [mPa·s (20 °C)]**	**Dielectric constant [ε_r]**	**Electrical cond. [S/cm]**	**Density [g/cm³]**	**Surface tens. [mN/m]**
PVA	N.A.	10	$1.63 \cdot 10^{-12}$	1.19 - 1.31	N.A.
Mineral Oil	25 - 80	2.2	$1 \cdot 10^{-14}$	0.85	31
Water	1	80	0.5–1000 $\cdot 10^{-6}$	1.00	72
Glycerol	1400	46.5	$6.4 \cdot 10^{-6}$	1.261	64
Cool 2 fluid	N.A.	N.A.	N.A.	N.A.	N.A.
Glycerol-Water 30/70	2.5	54	N.A.	1.06	67
PVA-Water 20/80	4–6	54 (frequency-dependent)	$4.4 \cdot 10^{-6}$	1.05	N.A.

Table 4.2: Physical properties of the analyzed liquids

Changed variables between each experiment included:

- Microscope slide distance from the LiNbO3 crystal.
- Voltage supplied to the Peltier
- Liquid used
- Droplet dimension

Each variable was modified inside the range described in Tab 4.3, while keeping the other constant to isolate the effect of each variation.

Variable	**Values / Range**	**Unit**
Liquid type	Glycerol-Water, Mineral oil, Cool 2, PVA-Water	/
Substrate distance	1 - 5	mm
Droplet volume	5 – 8	µL
Applied potential	1.5 – 2.0	V

Table 4.3: Summary of the experimental variables varied independently.

The results from these tests were positive and for the first time a pyroelectric jet was successfully recorded in video. Below, a few screenshots from the micro-camera that show the Taylor cone formation.

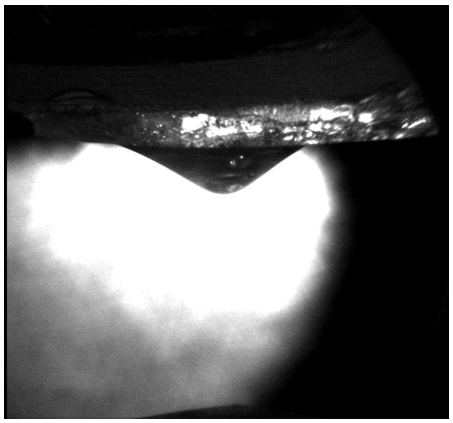

Figure 4.10: Taylor cone formation with mineral oil

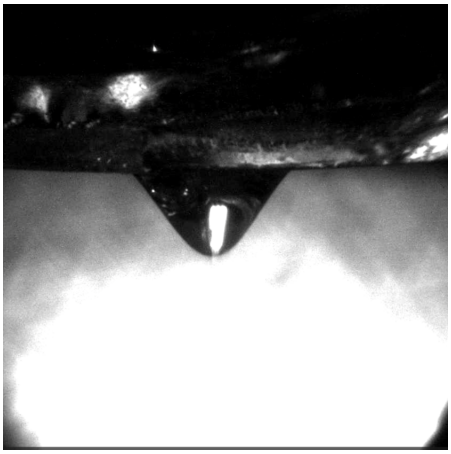

Figure 4.11: Taylor cone formation with COOL 2 liquid

4.4.2 Replicated test setup with flux sensor

After gaining confidence with the testing reproducibility conditions, the previously seen configuration was replicated using the flux sensor brought from Polito as the heat source. The setup remained the same with some slight changes:

- Temperature control through an Arduino board coupled with a type K thermocouple

- Test carried out both in attractive and repulsive configuration

The testing procedure remained alike the previous one except that, thanks to the temperature control, now the heating phase of the crystal was always stopped when reaching 60 °C. A typical temperature profile can be seen in Fig 4.12 below. Tests performed in attractive configuration gave the same results as in the previously analyzed case. However, the greatest difference was represented by the reversed jetting direction obtained in the latter tests. The droplet, instead of being attracted from the slide glass to the crystal, was positioned above the crystal on top of the hydrophobic PDMS substrate and in this case jetted towards the slide glass.

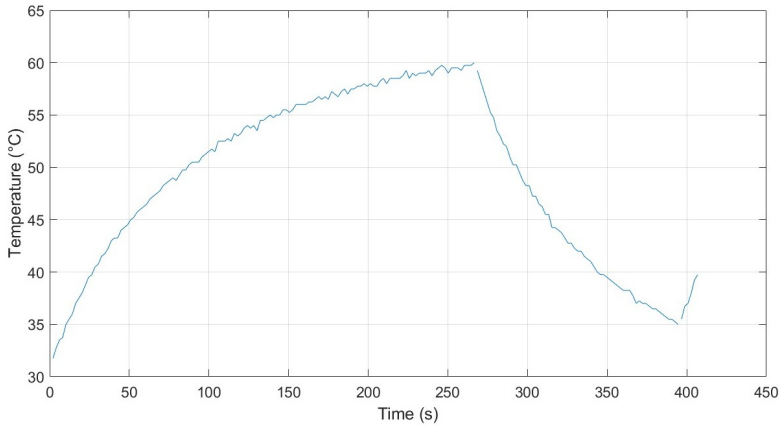

Figure 4.12: Tipycal testing temperature vs time profile

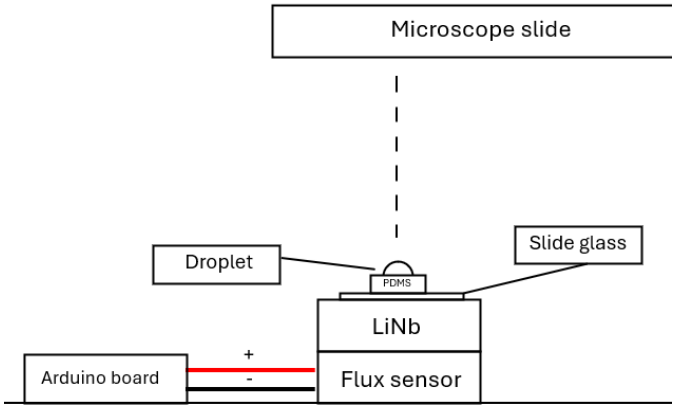

Figure 4.13: Schematic of repulsive setup at CNR Isasi with various components

4.4.3 Results achieved at CNR

At the end of the two-week period, the research done at the CNR Isasi was successful and provided a lot of useful results for comprehension and reproducibility of the effect.

Firstly, a clean pyroelectric effect was obtained in a brand new testing setup mounted from scratch: the majority of tests were conducted with the flux sensor as a heat source with temperature control programmed in Arduino.

Mineral oil is confirmed to be the most reactive liquid. Among all the tested fluids, only the mineral oil got to experience an actual detachment of the fluid from the Taylor cone with a jetting, while the others were only able to form the

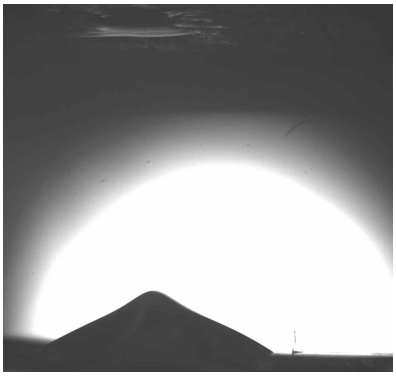

Figure 4.14: Video frame of Taylor cone in repulsive configuration (mineral oil)

cone and produce a pulsating-like movement. Looking at Tab 4.2 this result can be attributed to its low values of surface tension as discussed in section 4.1.

Among all the modified variables, a direct relationship between the glass slide distance from the crystal and the magnitude of the jetting was found. However, this topic will be analyzed more deeply later in this chapter.

The repulsive configuration seen in the last tests represented an important step forward since there was no recorded evidence of such a configuration being realized against gravity. This liquid motion against gravity works the best with the objective of the thesis: the cooling device forced convection cycle would be easily implemented with a jetting of this type.

4.5 Effect characterization on working setup

With the knowledge acquired during the period at CNR, a whole new set of tests was possible in the SMALL lab in Turin. These tests had several objectives:

- Characterize the effect with known condition in a controlled environment for variable distance
- Obtain a first evaluation of the phenomena heat transfer value
- Design some kind of 3D printed substrate aimed to induce a multi-jet
- Test the effect for a constant temperature heating

4.5.1 Study of distance dependency

The first goal was to reproduce a working setup in the SMALL lab by applying what was understood at the CNR. A similar testing workbench was built and after a few tests a pyroelectric jet was obtained without any big problem. Below, Tab 4.4 shows the main features of the adopted setup.

Camera model used	https://it.rs-online.com/web/p/microscopi/1964075
Ambient temperature	23 °C
Droplet volume	2 μL
Working fluid	Mineral Oil
Temperature profile	Heating from 30/35 to 60 °C and cooling down to 45 °C
Configuration	Heat source, Niobate, Glass slide, PDMS, Drop, Target slide
Heat source	Commercial 1 cm^2 polyimide resistor
Liquid drop replacement	Every glass slide distance change
Applied potential difference	9 V
Current through resistor	0,322 A
Power delivered to resistor	2,9 W
Crystal face used	Z -

Table 4.4: Setup condition adopted for SMALL lab testing

The next objective was to obtain a characterization of the effect for a variable distance while maintaining the other properties known and constant. The droplet was collected with a precision pipette of 2 μl volume and positioned on the PDMS hydrophobic substrate brought from CNR laboratory.

A 3D printed geometry was used to maintain precise distances between the droplet base and the target slide glass. The piece was designed by measuring all heights of the setup components, then these values were given to SolidWorks. The piece, which can be seen in Fig 4.15, 4.16, consisted of a stand for the slide glass with gaps separated by a known distance of 2 mm.

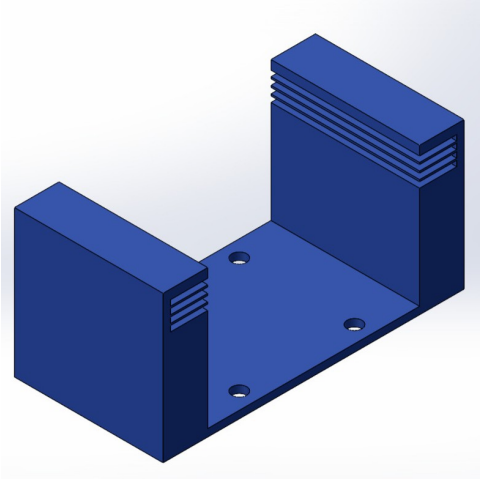

Figure 4.15: Support SolidWorks view

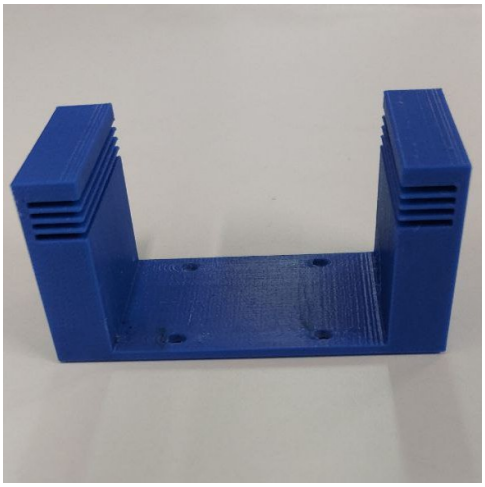

Figure 4.16: Support frontal picture

By positioning the slide glass on the stand above the droplet, the distance was known: values span between 5 mm and 1 mm; this was possible by using another small piece of 1 mm thickness put below the printed geometry to reduce the distance when needed. Thanks to this configuration, several tests had been made that showed a direct correlation between the distance of the target slide glass and the frequency of the jetting phenomena.

A post-processing software called Fiji ImageJ was used to analyze the recorded videos. A rectangular area of interest was defined, and the software recorded when the pixel changed color in that area. This technique was used to evaluate how many jetting phenomena occurred in a certain time span. The jetting was recorded in a graphic with frames as abscissa and number of changing pixels as ordinates Fig 4.17. By counting the number of peaks present in the graph, an estimate of frequency was possible.

The frequency was evaluated as follows:

$$Frequency[Hz] = \frac{N.of Peaks}{time[s]} \tag{4.1}$$

While the time interval is equal to:

$$time[s] = \frac{N.of Frames}{VideoFrameRate[FPS]} \tag{4.2}$$

From these data, a linear trend can be extracted, shown in the Tab4.5.

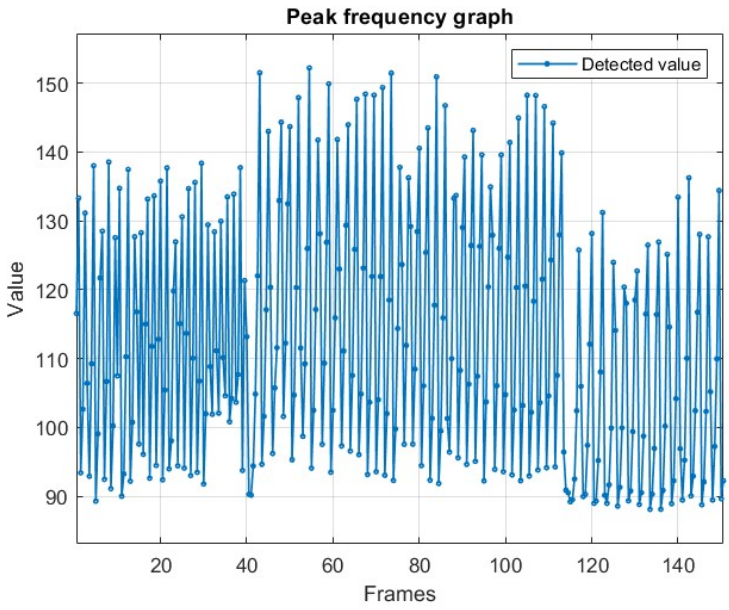

Figure 4.17: Jetting frequency graph example

Distance [mm]	N of frames	FPS	Time [s]	N of peaks	Frequency [Hz]
1	50	12	4.167	12	2.88
2	50	12	4.167	11	2.64
3	200	12	16.67	10	0.60
4	100	12	8.33	4	0.48
5	No jetting	\	\	\	0

Table 4.5: Measured peak frequency at different pipette-substrate distances.

Results show how, for smaller distances 1-2 mm, the jetting has higher values of frequency, almost 3 Hz, while when the distance increases and reaches 3-4 mm the frequency experiences a reduction to values of less than 1 Hz. In addition, with the working condition shown above, the jetting stops for 5 mm distances or more. The variation in frequency is also characterized by different dimensions of the Taylor cone: the higher frequency corresponds to smaller jetting events with lower volume droplets, whereas as the frequency diminishes, the ejected volume increases, and the Taylor cone includes a larger portion of the droplet Fig 4.22, 4.23.

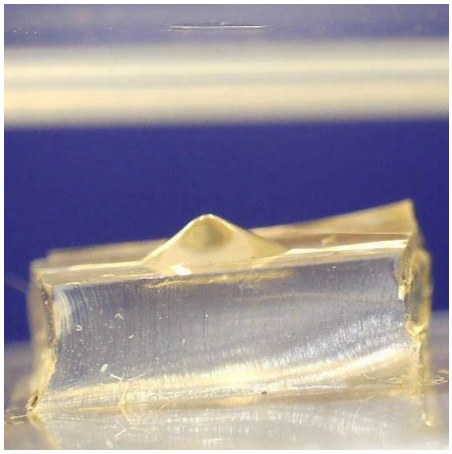

Figure 4.18: Taylor cone formation 3 mm distance

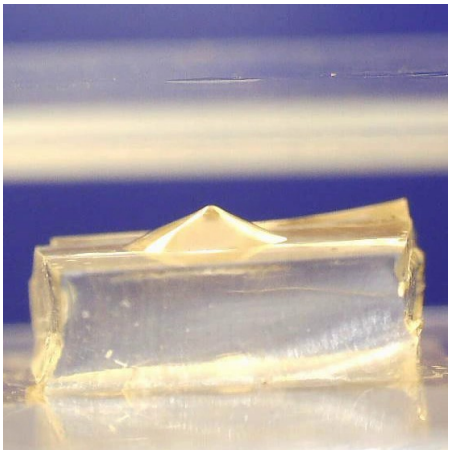

Figure 4.19: Taylor cone formation 2 mm distance

The dependency just seen can be explained by looking at the pyroelectric voltage formula seen in chapter 2. The target glass slide, indeed, functions as the lower plate of a virtual capacitor, inducing the electric field across the gap. This electric field will be inversely proportional to the distance between the glass slide and the base of the droplet from the equation:

$$E_{pyro} = \frac{P \cdot d}{\epsilon_0 \cdot \epsilon_r \cdot d_{target}} \tag{4.3}$$

So, a simple way to enhance the effect is to reduce this distance until the electric field is enough to produce a jetting phenomenon, with a lower limit related to the droplet dimension. However, as the distance reduces, the stronger field tends to affect the top liquid particles strongly, leaving the rest of the droplet behind, reducing the liquid jetting volume as the distance becomes smaller.

4.5.2 Heat transfer evaluation

To have a complete overview of the feasibility of the effect for cooling purposes, an estimation of heat flux carried by the droplet jetting has been done. These measurements were performed on the setup already seen for the variable distance setting, at a slide glass distance of 3 mm. 3 mm is the distance with the highest mass transport, due to good frequency and bigger dimension of the Taylor cone. The heat flux was determined from the formula:

$$HeatFlux = \frac{m_{fluid} \cdot cp_{fluid} \cdot (T_{fluid} - T_{target})}{t \cdot S} \tag{4.4}$$

- m_{fluid} - represent the mass of fluid transferred from the droplet to the target in a certain time [Kg]
- cp_{fluid} - the specific heat of the working fluid used for the jetting $[J/Kg \cdot K]$
- T_{fluid} - the temperature at which the fluid experience the jetting [°C]
- T_{target} - the temperature of the target slide glass where the hot fluid is jetted to [°C]
- t - the time interval in which the fluid mass is transferred [s]
- S - the heat exchange surface considered, in this case the choice is the top face of the pyroelectric crystal $[m^2]$

Due to the small size of the droplet, measuring the mass was not an easy task.

First measuring attempt involved a precision weight with a resolution up to 0,001 g. Several measurements of the slide glass and of the PDMS substrate were made before and after the effect was triggered. In Tab 4.6 a summary of the various masses of the components. However, the dimension of the base droplet was already

	Weight [g]
Empty glass	4.596
PDMS substrate first case	0.295
PDMS substrate first case with 2 μl droplet	0.297
PDMS substrate second case	0.878
PDMS substrate first case with 2 μl droplet	0.880

Table 4.6: Setup components masses review

near the resolution limit of the weight: a mineral oil droplet of 2 μl weights around 0,0015 g. So, the portion of the droplet that experienced the jetting phenomena was not enough to show any change on the weight display.

Another strategy was to post-process the recorded video and extract the mass of the fluid on the slide glass from a volumetric estimation. The PDMS substrate has been used as a known reference of 2 mm to evaluate the diameter of the fluid droplet accumulated on the target. From Fig 4.20 can be seen that the diameter of

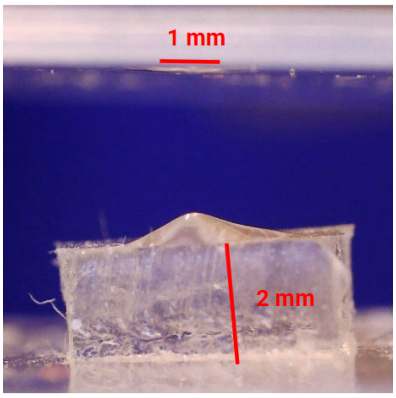

Figure 4.20: Video-frame to extract transferred liquid volume. It is possible to see the PDMS reference measuring 2 mm and the droplet with a diameter of 1 mm.

the droplet is around 1 mm. This diameter was then used to estimate the volume from the sphere volume formula:

$$V = 4/3 \cdot \pi(d/2)^3 \tag{4.5}$$

The obtained volume is 0,5 μl, a quarter of the starting droplet.

From the Temperature vs Time graph, Fig 4.21, more data can be extracted:

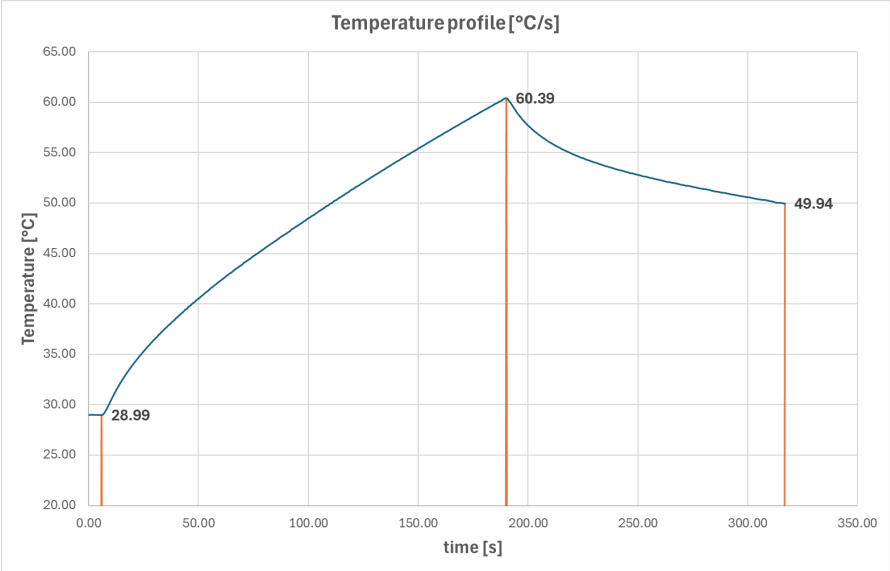

Figure 4.21: Temperature profile adopted for heat flux estimate with a 3 mm distance

- Looking at the video, the jetting phenomena to accumulate the 1 mm diameter droplet lasts 50 seconds
- The medium temperature of the liquid during the jetting is 50 °C
- The target temperature can be approximated equal to ambient: 23 °C

Remembering the mineral oil properties listed in the table below.

Mineral oil properties	**Value**
Viscosity (20°C)	25–80 mPa · s
Dielectric constant (ϵ)	2.2
Electrical conductivity	1×10^{-14} S/cm
Density	0.85 g/cm^3
Surface tension	31 mN/m
Specific heat	2 kJ/(kg · K)
Thermal conductivity	0.132 W/(m · K)

Table 4.7: Physical properties of mineral oil.

The mass is obtained by multiplying the droplet volume times mineral oil density: $4{,}25 \cdot 10^{-7} Kg$.

A first evaluation of the power transferred returns a value of $\dot{Q} = 4{,}59 \cdot 10^{-4} W$. Considering as the exchange surface the LiNb crystal base area of 1 cm^2 the heat flux will be $\dot{q} = 4{,}59\, W/m^2$. Since the temperature difference is known, from the convective heat transfer formula an estimation of h can be done:

$$h = \dot{q}/\Delta T = 0{,}17\, W/m^2 K \tag{4.6}$$

Comparing this h value with the values found in literature for natural convection (h = 5 ÷ 25) the heat transfer is not enough for cooling purposes.

4.5.3 Multi-jet geometry testing

A possible solution to enhance the cooling power has been investigated: testing a multi-jet configuration that enables the formation of multiple Taylor cones at the same time. Two different experimental setups were put to test:

- Multiple jets generated by individual droplets deposited on separate substrates, in a configuration similar to the one previously described.
- Multiple jets originating from the same liquid reservoir, geometrically separated by a 3D-printed mask designed to promote the formation of distinct Taylor cones.

- Separate substrates case First tests were conducted on this configuration due to simplicity in realizing the setup and to ensure that a multi-jet was possible before starting to work on the new configuration.

Experimental parameters were the same seen in Tab 4.4. However, just a few tests to validate the effect were carried out at a fixed distance of 2 mm. From the figures below, it can be seen that the experiment succeeded in obtaining both a double and a triple jetting from separated substrates.

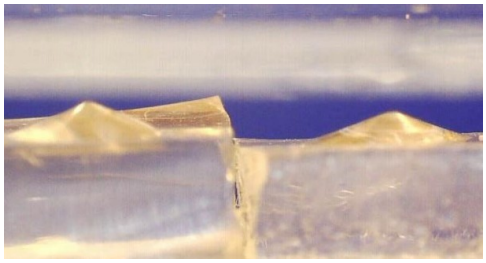

Figure 4.22: Double jetting experiment

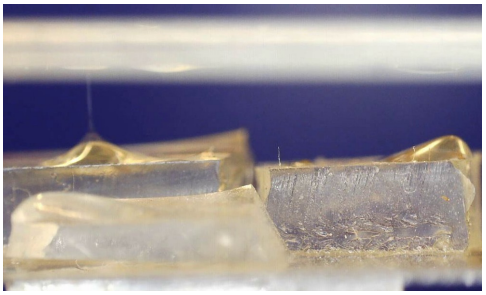

Figure 4.23: Triple jetting experiment

This setup, though, remains of low interest due to the difficulty in reproducing it in cooling devices or in general in a real scenario outside of testing procedures.

- Single reservoir case The previous results encouraged work on the single reservoir concept, since it has the capability to be implemented in future applications for increased heat flux. Several differences characterize the single reservoir setup with respect to the one previously seen:

- A bigger pipette has been used to fill the whole reservoir that needs to feed more than one Taylor cone
- The jetting phenomena is induced by 3D printed geometries modeled with features that tend to give the liquid reservoir a conical shape
- In this case the 3D printed substrate is placed directly on the crystal without the need to have a hydrophobic PDMS

Below, some figures of the printed geometry trials that gave negative results: the fluid stayed still or simply moved along the surface plane.

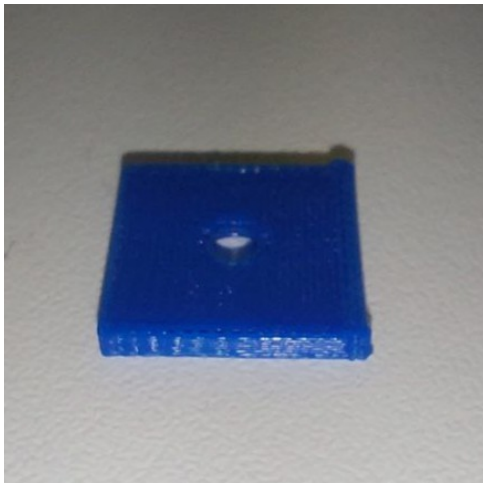

Figure 4.24: 1 st geometry

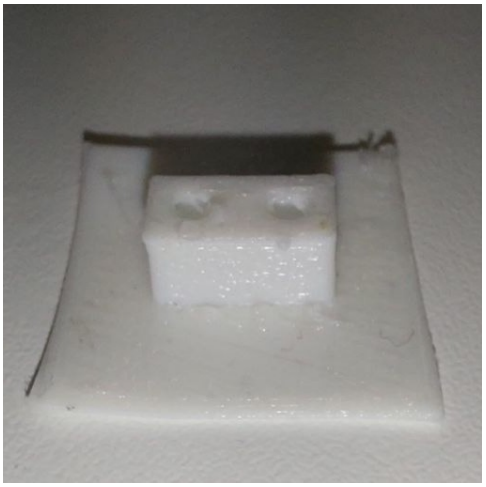

Figure 4.25: 2 nd geometry

After dozens of attempts, mostly realized with the Ultimaker 3 printer, the first working geometry was found. Main features of this geometry included: two conical tips with the task of forming the liquid pool for jetting, a shared liquid reservoir below with a known volume, the usage of hydrophobic TPU to increase as possible the liquid contact angle.

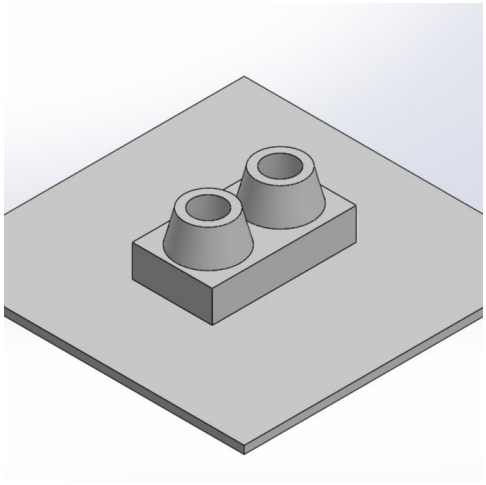

Figure 4.26: Working geometry SolidWorks view

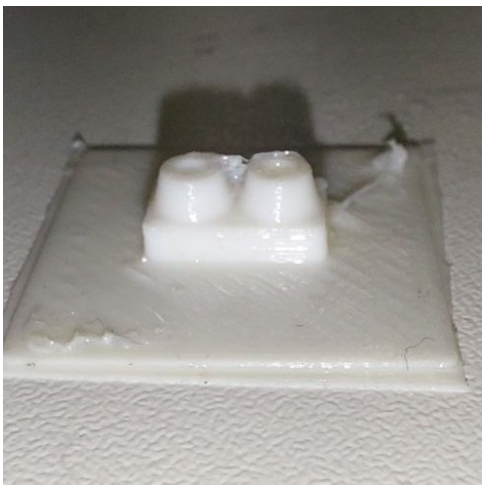

Figure 4.27: Working geometry picture

While maintaining the same working conditions, with this geometry, a double contemporary jet was obtained. The phenomena manifested clearly at small distances 1-2 mm. Here, one video frame where the double Taylor cone is visible.

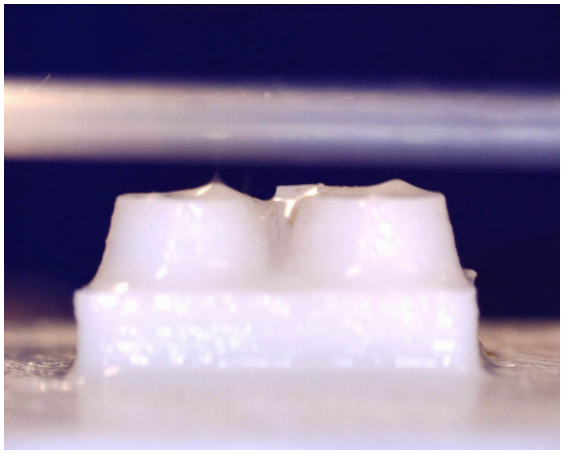

Figure 4.28: Double Taylor cone from same reservoir

Results demonstrate that a multiple pyroelectric jet from a single liquid reservoir is possible and, with proper and more comprehensive research, the number of contemporary jets could be incremented to interesting numbers.

4.5.4 Steady state temperature tests

The experimental procedure carried out till now exploited an induced temperature rise, as it was seen in the literature articles in chapter 2. However, in an actual cooling situation, the heat source would remain at a fixed temperature and the goal of the cooling device consists in shifting the equilibrium temperature to a lower value by increasing the heat transfer. Said so, to reproduce a constant temperature condition a few tests have been done to investigate the behavior of the pyroelectric crystal in this situation.

To simulate the constant temperature condition, the flux sensor was heated with constant power till it reached the thermal equilibrium asymptote with natural convection. LiNbO3 crystal was placed on top of it for the whole heating duration to ensure that even its temperature was stationary following the copper sensor thermal profile.

Below Tab 4.8 shows the main features of the heating setup. From the charts, it is possible to visualize the temperature trend and the asymptotic behavior reached after 3000 seconds. This condition verifies because, as the temperature difference increases, the heat released through natural convection goes higher till it equalizes the heating power of the power supply net of losses.

$$V \cdot I = h \cdot A \cdot \Delta T \tag{4.7}$$

At the 3000 s time the asymptote was almost reached and the temperature

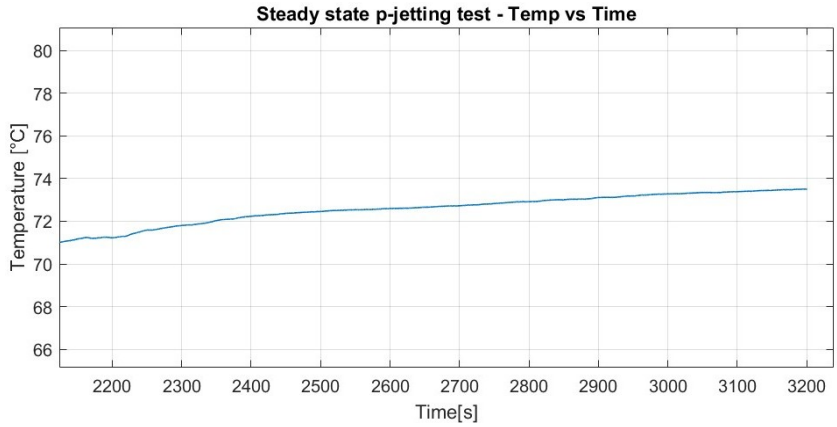

Figure 4.29: Last portion zoom of the Temperature vs time graph for steady temperature testing

Steady state temperature test	
Potential difference	6 V
Current	0,215 A
Asymptote temperature	73,5 °C
Ambient temperature	23 °C
Time to steady state	3000 s

Table 4.8: Working condition for steady state temperature tests

change rate was lower than 1 degree for 500 seconds. At that point, the liquid droplet was placed on top of the crystal together with the PDMS substrate and the target slide glass. However, the crystal did not produce any electric field and the liquid stayed still, not showing any sign of interaction.

To obtain a clearer picture of the crystal thermal profile, two simulations have been carried out on the MATLAB PDE tool. The simulations show the temperatures distribution in the crystal section in thermal equilibrium and for a dynamic temperature evolution in time.

- Thermal equilibrium simulation In this simulation, the PDE modeler of MATLAB has been used to recreate the cross-section of the crystal heated at a constant temperature in thermal equilibrium. The domain has been defined as a rectangular surface with a base of 10 mm and height of 2,5 mm. The following boundary conditions have been implemented on the mesh to obtain the solution:

- Dirichlet on the hot border: $T_{hot} = 73{,}5°C$
- Robin on air facing border: $h = 10\,W/m^2K$, $T_{amb} = 23°C$

- Adiabatic vertical boundaries: $\frac{\delta T}{\delta n} = 0$
- Thermal conductivity of LiNbO3: k= $5\, W/mK$

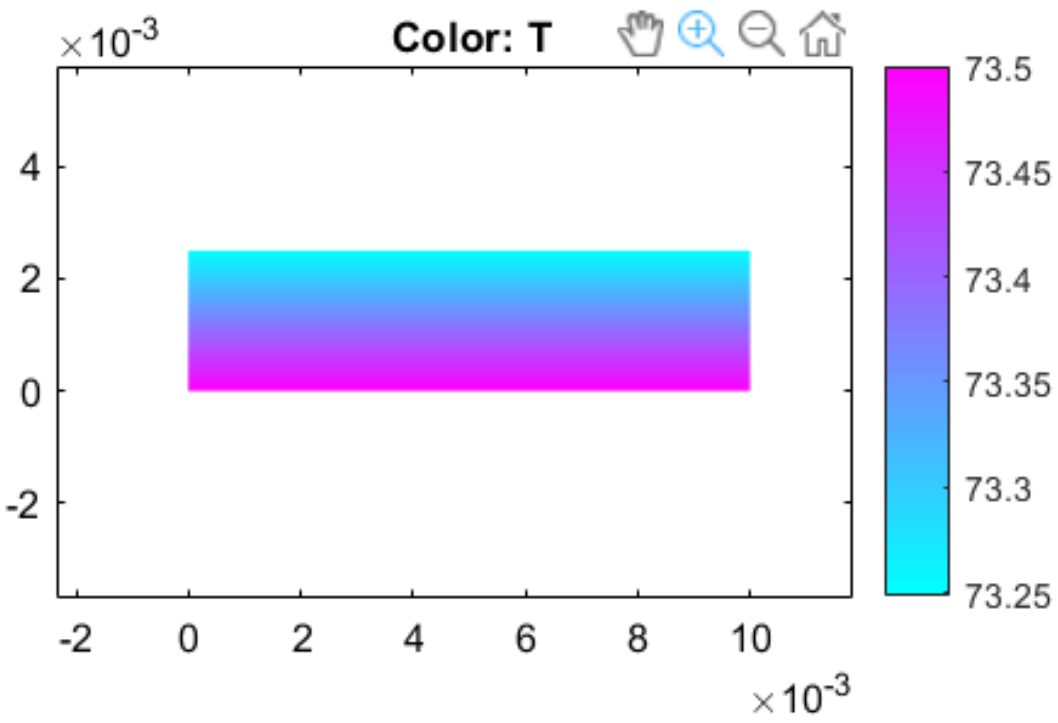

Figure 4.30: Constant temperature PDE modeler simulation

Looking at the solution Fig 4.30 the temperature distribution inside the crystal appears almost constant. The temperature difference between the opposite faces doesn't exceed 0,25 °C. The almost uniform temperature is imputable to the high thermal conductivity of the crystal and its small thickness.

- Dynamic evolution in time Additionally, a dynamic thermal simulation has been conducted on the MATLAB PDE tool to analyze the temperature distribution inside the crystal during the usual testing scenario.

To recreate the testing conditions, the same geometrical domain was set with similar boundary conditions. The major difference was the imposition of a variable temperature with a logarithmic trend on the hot face of the crystal. This temperature evolution resembles the heating ramp needed by the LiNbO3 to produce a pyroelectric jetting in our setup. Figures 4.31, 4.32, 4.33 give an overview of the simulation results.

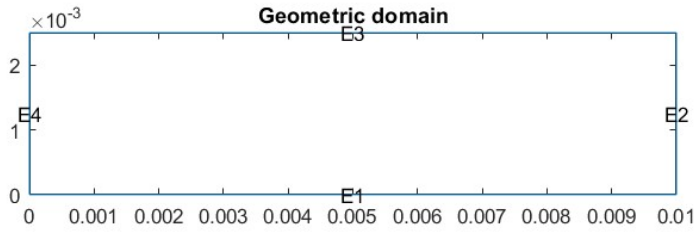

Figure 4.31: Geometric domain for the simulation

The dynamic simulation shows a temperature spatial gradient with a maximum of 1 °C built at the start of the heating that tends to the stationary value shown in the previous simulation of 0,25 °C.

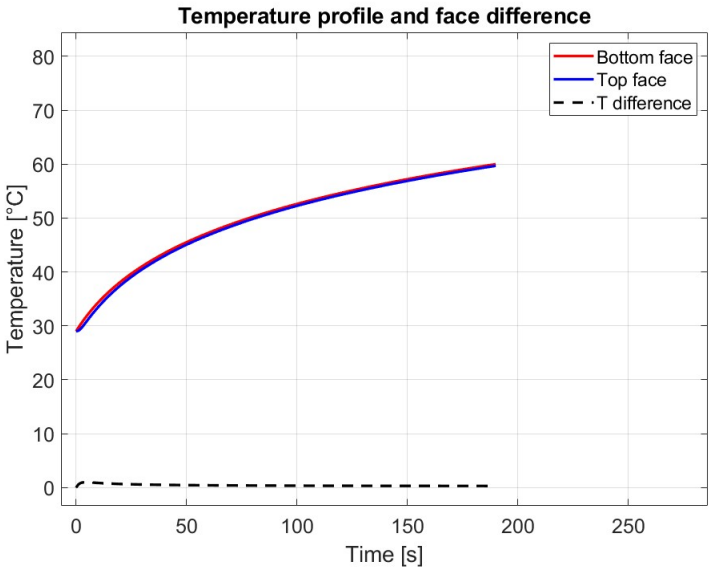

Figure 4.32: Overview of simulation temperature

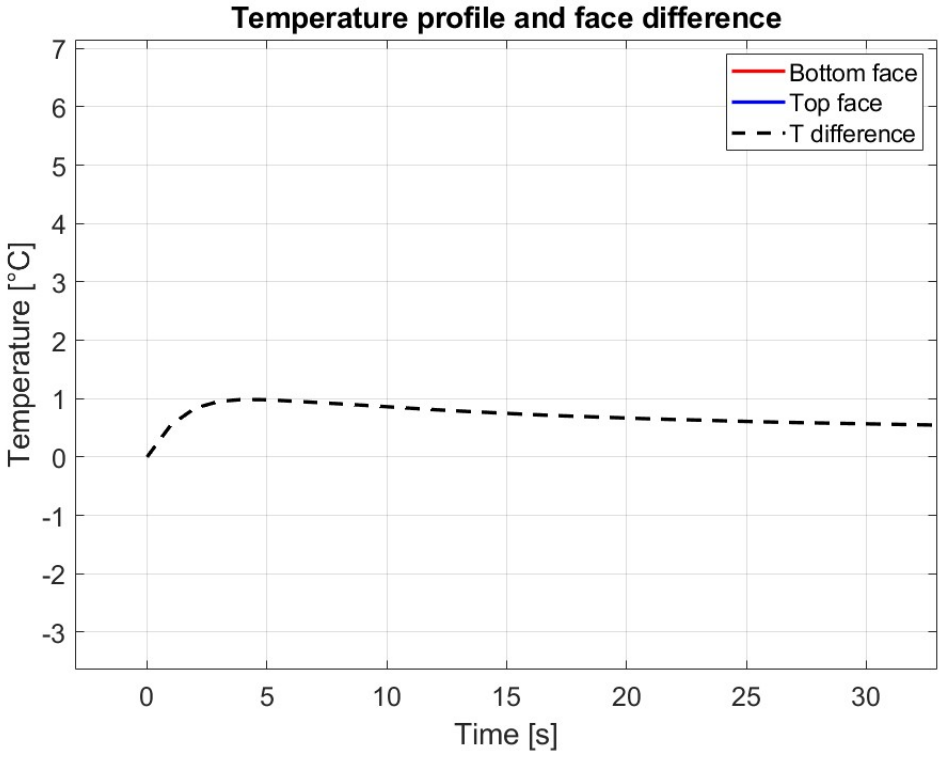

Figure 4.33: Zoom in on temperature difference

From the two simulations, the spatial thermal gradient remains inconsistent in both cases. Nonetheless, the empirical results had totally different outcomes with a visible and continuative effect in the dynamic case, with respect to the stationary one. Following these results, after checking the literature, no recorded dependency was found between the pyroelectric potential and a spatial temperature gradient. Only a temperature gradient in time can produce a charge accumulation on the crystal, while the spatial temperature gradient has no effect. This implies that without an active temperature modification of the crystal, the p-jetting cannot take place.

Chapter 5

Results and Future Perspective

5.1 Results acquired summary

In the following section, a review of the obtained results will be displayed with the relative inferences.

- Optimal condition to obtain a Pyroelectric jetting Firstly, an in-depth study on the best conditions to grant reproducibility for pyroelectric jetting has been done. To recreate an optimal setup with the formation of an EHD induced Taylor cone a set of rules must be followed:

- **Liquid volume**: the amount of liquid must be selected wisely fitting the dimension of the substrate. A too large amount of liquid requires a stronger electric force to be moved. Moreover, a greater liquid mass tends to spread over the surface rather than forming a spherical shape, due to the influence of gravity.

- **Droplet contact angle**: to drive the liquid toward forming a Taylor cone, the contact angle should be as high as possible. To deal with this a hydrophobic PDMS layer has been used for the experimentation. However, other alternatives are still viable, such as, surface coatings or substrate geometries that induce a conical shape of the liquid reservoir.

- **Presence of a target**: a target put at a certain distance from the pyroelectric crystal works as a capacitor plate. Without the target, the pyroelectric voltage is not able to produce an electric field, and as a result the p-jetting is impossible.

- **Video evidence**: as demonstrated in the thesis, due to the scale and peculiarity of the effect, recorded videos with micro-cameras are essential to obtain a clear understanding of what is happening.

- Novel repulsive configuration Then a novel jetting configuration was tested. For the first time, repulsive jetting from the crystal toward a slide glass has been recorded against gravity. The scheme in Fig 5.1 is intended to visualize the experimental setup with the various components to produce this kind of result. This constitutes important evidence, as this kind of configuration works the best

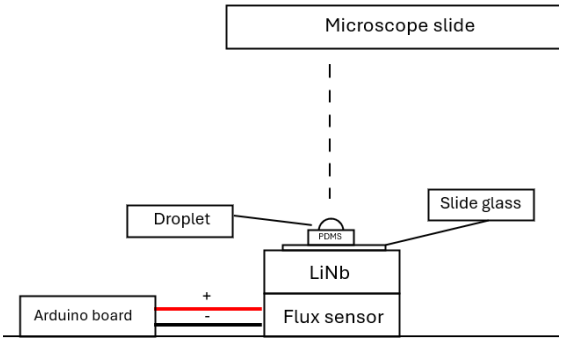

Figure 5.1: Schematic of repulsive setup against gravity

for cooling purposes: the pyroelectric crystal needs to be in contact with the heat source to produce a potential. If the liquid is placed in a reservoir above the crystal, thanks to p-jetting, the heated fluid moves away with the possibility to be cooled in a heat exchanger and close the cycle back in the reservoir. The discussed convective cycle can happen if taking advantage of the gravity that pulls the liquid back to the starting reservoir which otherwise would need another method to be replenished. Since this configuration is of relevant interest for the thesis topic, all the subsequent results will be focused on this repulsive setup against gravity.

- Target distance linear relationship Another important evidence acquired in this thesis project is the direct relationship that exists between the presence and distance of a target, in our case a microscope slide, positioned above the crystal and the magnitude of the effect. In particular, the slide glass distance directly affect the electric field from the equation 4.3. From video and testing evidence, a lower distance between the slide glass and the crystal produces an increase in the jetting frequency that grows linearly as the distance decreases Tab 4.5. This suggests that a stronger electric field tends to affect more the liquid particles, reducing the time to form the Taylor cone shape and produce the jet. However, with the frequency increases a lower portion of the liquid is involved in the jetting process and, as a

consequence, for very small distances, the jetted volumes tend to grow smaller. In addition, when the 1 mm distance threshold is surpassed, the liquid forms a bridge that connects the two sides, making the jetting phenomena unfeasible.

- Cooling power estimate The heat flux estimation showed that in the actual testing configuration, the cooling capacity of the jetting phenomena is still severely below the natural convection values. The liquid volumes involved are not sufficient, and in the testing conditions adopted, bigger volumes result in no or inconsistent jetting. However, the jetting phenomena is proven to remove heat in a precise way while keeping a sufficient air layer to separate thermodynamically the two surfaces. Furthermore, the heat flux is potentially scalable by working on fluid properties and jetting flow rate till the reach of satisfying heat transfer values.

- Multi-jet proof of concept Through 3D printing and several failed attempts, a proof of multi-jetting from the same liquid reservoir was obtained. The recorded videos showed how the electric field was capable of producing multiple contemporary Taylor cones. The necessary condition to obtain such a result is providing the liquid a pool with a shape that encourages the conical shape. In addition, such a geometry must not interfere with the electric field and needs to guarantee, depending on the liquid, a decent contact angle for the droplet. The figures 4.28 taken from the recorded videos show how the multiple effect maintains the same magnitude of the single jet while shooting double the amount in the same time.

- Thermal gradient review Through the experimental testing and numerical simulation of the temperature inside the crystal, a complete understanding of the thermal gradient needed to produce the effect was obtained Fig 4.30, 4.32. In the literature, a temperature over time gradient was described [39], but the possibility of a spatial gradient between the faces was investigated. However, after several trials, the empirical results confirmed the literature, and the effect only happened when a temperature changing in time was present. This excludes the passive cooling scenarios from the p-jetting application, except for particular cases where the temperature naturally oscillates or reaches high values for brief time intervals.

5.2 Future research possibility and limits

Now, a section will be dedicated to the future potential of the pyroelectric jetting as a cooling method and the thermodynamic limits for future application or research. The p-jetting in itself is a very promising effect and, with adequate research, could represent an interesting addition in the power electronics cooling panorama.

5.2.1 Thermodynamic limit evaluation

A preliminary study can be carried out by confronting the thermodynamic limit of the system with the actual power needed to perform the p-jetting phenomenon.

The upper limit is represented by the Carnot exergetic power between the two temperatures the crystal is working in between: the hot surface temperature and the target temperature, which can be approximated to the ambient one. The exergetic power is found from the formula:

$$\dot{L_{ex}} = \dot{Q_{in}} \cdot (1 - \frac{T_{cold}}{T_{hot}}) \tag{5.1}$$

- $\dot{Q_{in}}$ - heating power supplied to the crystal by the electric battery net of losses [W]
- T_{cold} - Ambient temperature = 23°C
- T_{hot} - Max temperature at which the jetting phenomena manifest = 60 °C

The heating power supplied to the crystal is obtained from:

$$\dot{Q_{in}} = \frac{m \cdot cp \cdot \Delta T}{\Delta t} \tag{5.2}$$

- $\Delta T = 30$°C
- cp - specific heat of the LiNb = 648 $J/Kg \cdot K$
- m - mass of the crystal evaluated with density and volume = 1.16 g
- Δt - time to heat up the crystal till max temperature = 190 s

$\dot{Q_{in}} = 0{,}11\, W$

By putting all the right data in the Exergetic power formula Eq 5.1 with the temperatures in kelvin:

$$\dot{L_{ex}} = 0{,}11 \cdot (1 - \frac{296{,}15}{333{,}15}) = 12{,}2\, mW \tag{5.3}$$

So, from the Carnot coefficient, with these temperatures, less than 10% of the supplied heat can be exploited as exergetic power.

Now the actual power exploited by the p-jetting must be estimated to confront it with the upper limit. In general, the two main work-consuming phenomena are the atomization of the liquid reservoir into smaller droplets and the shooting against gravity of the ejected droplets. Both contributions will be evaluated:

- Atomization power estimate From the literature [46],[47] the atomization power depends on the surface tension of the chosen liquid and on the area of the droplet formation. In numbers:

$$\dot{W_{atom}} = \frac{\gamma \cdot A_{droplets}}{\Delta t} \tag{5.4}$$

- γ - surface tension of mineral oil = 30 mN/m
- $A_{droplets}$ - total external surface of ejected droplets
- Δt - time interval to shoot the whole droplet volume = 50 s

To calculate $A_{droplets}$, an estimate of the number of ejected droplets and their size is necessary. Assuming 50 droplets are ejected to transfer a volume of 0,5 μl, their radius would be 136 μm. With this radius, the area of a single droplet can be calculated as $A_{droplet} = 2{,}32 \cdot 10^{-7} m^2$ and then multiplied by 50, the number of droplets.

$$A_{droplets} = 2{,}32 \cdot 10^{-7} \cdot 50 = 1{,}16 \cdot 10^{-5} m^2 \tag{5.5}$$

With this, the value of the atomization power results:

$$\dot{W_{atom}} = \frac{0{,}03 \cdot 1{,}16 \cdot 10^{-5}}{50} = 6{,}96 \cdot 10^{-9}\, W \tag{5.6}$$

- Droplet gravitational power In the novel configurations adopted in this thesis, the droplets are ejected against gravity, so a component of the power available is employed to win the gravity. This power is simply evaluated as follows:

$$\dot{W}_g = \frac{m \cdot g \cdot h}{\Delta t} \tag{5.7}$$

- m - mass of the total ejected volume of 0,5 $\mu l = 4{,}25 \cdot 10^{-4} Kg$
- g - gravitational acceleration = 9,8 m/s^2
- h - the height difference between the base of the droplet and the slide glass = 3 mm (intermediate distance considered)
- Δt - time interval to shoot the whole droplet volume = 50 s

The gravitational power will be: $W_g = 2{,}5 \cdot 10^{-7}\, W$

- Power values comparison Now, by summing the two powers previously evaluated, the total exergy consumed by the process is found:

$$\dot{L_{ex}} = 2{,}5 \cdot 10^{-7} + 6{,}96 \cdot 10^{-9} = 2{,}57 \cdot 10^{-7}\, W.$$

This value can be confronted with the total Carnot exergy available seen before to make an estimation of the losses and how much the p-jetting is theoretically improvable. The exergy exploited by the p-jetting is below 0.01 % of the total, meaning the process still needs to be investigated and researched in order to reach the optimum, while the thesis obtained results can be considered a good starting point.

5.2.2 Future improvements consideration

From the thesis work, several paths can unleash to carry on the research conducted on pyroelectricity cooling applications and p-jetting phenomenon. Future experimentation on the effect should be pursued with the goal of improving the magnitude and reproducibility of the p-jet effect. To do so, a review of the most critical aspect that would need further research:

- Working liquid As first research topic, there is the working liquid. In the thesis, among the tested liquids, mineral oil had the best response to the pyroelectric field. Mineral oil is characterized by low surface tension and is a complete dielectric with a very low ϵ value. However, only four, between liquids and mixtures, were tested consistently and a lot of possibilities remain undiscovered. An example is the addition of surfactants to lower the surface tension of other liquids, even the already tested ones, to see how they would react reducing their surface tension. Other than that, a deeper study of dielectric oils could be conducted: since the mineral oil worked well, an insight in that liquid category would be beneficial, testing which reacts better in our experimental conditions.

- Substrate geometry The geometry below the droplet is another topic that still needs to be investigated in order to reach the optimum. For the thesis, the best reproducibility has been obtained with a PDMS hydrophobic surface positioned on a slide glass on top of the LiNbO3 crystal, but other possibilities could be viable or even better. As seen for the multi-jet 3D printed geometry, having a substrate with a conical shape ease the Taylor cone formation while, if acting on a single reservoir induces the formation of multiple p-jets. Exploring the various geometries and materials for the substrate could bring benefits both for the p-jetting effect magnitude and amount of jetted liquid, but even for having a jetting a matrix that

exploits the whole surface of the crystal. Here, a possible design idea for the matrix jetting surface:

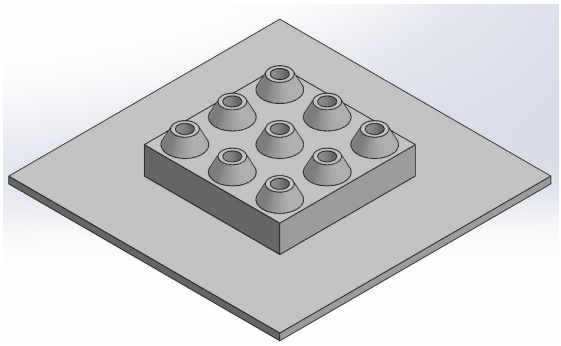

Figure 5.2: Possible design for multiple jetting matrix

- Active cooling or thermoelectric materials Lastly, empirical results, confirmed in the literature, show that for stationary situations, a passive cooling solution involving the p-jetting is not feasible. A possible alternative is exploiting the p-jetting with an external heating source that triggers the effect precisely when needed. A Peltier element could be used to trigger the effect both in heating and cooling, coupled with a temperature sensor to obtain the p-jetting only when the temperature exceeds a certain value. By working on an advanced substrate geometry, the liquid droplets could be directed exactly on the hot spots of the electronic chip at the right moment. In addition, this active cooling method would provide several advantages:

- Absence of moving mechanical parts
- No electric problems if coupled with a dielectric working fluid
- Noiseless device
- Possibility to scale it in arrays

Conclusions

The continuous evolution of power electronics devices has made thermal management an increasingly critical issue. The increase in power density, with the miniaturization of components, demands sophisticated and compact cooling solutions. Within this context, this thesis has explored the feasibility of using the pyroelectric effect, specifically the phenomenon defined as p-jetting, for electronics cooling. This innovative mechanism generates convective motion without the need for electrodes, nozzles, or any mechanical moving parts.

The main concept is to exploit the electric field generated by a pyroelectric crystal, subjected to a temperature change, in order to induce the formation of an ElectroHydroDynamic jet capable of transporting heat away from the source. Experiments were carried out using Lithium Niobate (LiNbO3) pyroelectric crystals, selected for their strong pyroelectric properties, and various fluids. Among them, mineral oil proved to be the best due to its low surface tension and fully dielectric nature.

The thesis work followed this order: after a brief introduction to the world of cooling by exploring the main heat transfer method, a review of the main cooling techniques was done. Each cooling method was described to understand the working principle, and an estimation of the usual heat flux and heat transfer coefficient (h) was given.

Then, pyroelectricity was reviewed by looking at the physics involved and the coefficient that regulates the phenomena. In this chapter, a brief description of the LiNbO3 crystal was given, while describing all the other classes of pyroelectric materials.

The testing methodology consisted in generating a reproducible pyroelectric liquid jetting and then characterizing its properties. The p-jetting was found to be quite difficult to reproduce, and the initial tests were not successful. After two weeks at the CNR Isasi of Naples with the experts, who for the first time manifested the p-jetting, the phenomenon was reproduced at Polito with a precise testing setup. The experimentation in Turin produced several results; in particular, a novel "repulsive" jetting setup, where the fluid moves against gravity, was validated and

showed promising behavior for potential future applications in thermal management devices. It was also observed that the distance between the crystal and the target surface had a linear influence on the jetting frequency.

However, the results obtained in terms of heat flux, approximately 4,59 W/m^2, and heat transfer coefficient, around 0,17 W/m^2K, were significantly lower than those of natural convection. This shows that, in the actual configuration, the p-jetting cooling concept is not yet suitable for practical implementation.

A possible tested solution consists in generating multiple jets to increase the heat transfer. After trying various 3D printed geometries, a double contemporary jetting from the same reservoir was obtained. This result could be a good starting point to increase the heat flux values by designing geometries with jets that exploit the whole crystal surface.

Lastly, by testing the crystal at a constant temperature, the system's dependence on transient thermal gradients emerged: the jetting phenomenon does not occur under steady-state temperature conditions. This makes continuous passive cooling unfeasible and calls for hybrid or active solutions, such as integrating Peltier elements, to dynamically modulate the crystal temperature in response to heat loads.

From the obtained results, pyroelectric jetting proved not feasible for the, firstly thought, passive cooling scenario. First, the heat flux evaluated in the laboratory is not sufficient to overcome the natural convection cooling, and the p-jetting needs a precise configuration to manifest. Second, the energy efficiency of the system is extremely low: less than 0.01% of the available exergy is converted into useful fluid motion work. This encourages research to obtain better coupling between the thermal stimulus and the electrical response of the material. The cooling values could be increased by working on the jetting flow rate and number of jets, through a deeper research into the working fluid, substrate geometry, and temperature control. Regarding the need for a temperature variation in time, the device design could be transposed to an active cooling scenario. The crystal heating would come from an external source, but the jetting would be better controlled in time and space, while keeping the advantages seen before.

In conclusion, while the thermal performance achieved does not yet surpass that of conventional technologies, this work has laid the basis for a novel cooling method exploiting pyroelectric materials. Pyroelectric p-jetting emerges as a promising direction for future research, particularly in microscale or embedded systems where compactness, silence, and maintenance-free operation are essential.

Bibliography

[1] Bas J. van Ruijven, Enrica De Cian, and Ian Sue Wing. «Amplification of future energy demand growth due to climate change». In: *Nature Communications* 10 (2019), p. 2762 (cit. on p. 1).

[2] Niravkumar Dhameliya. «Power Electronics Innovations: Improving Efficiency and Sustainability in Energy Systems». In: *Asia Pacific Journal of Energy and Environment* 9.2 (2022), pp. 71–80 (cit. on p. 1).

[3] Frede Blaabjerg, Florin Iov, Remus Teodorescu, and Zhe Chen. «Power Electronics in Renewable Energy Systems». In: *2006 12th International Power Electronics and Motion Control Conference*. 2006, pp. 1–17. DOI: 10.1109/EPEPEMC.2006.4778368 (cit. on p. 1).

[4] Muhammad Kamran. «Chapter 11 - Global status of smart grids». In: *Fundamentals of Smart Grid Systems*. Ed. by Muhammad Kamran. Academic Press, 2023, pp. 461–473. ISBN: 978-0-323-99560-3 (cit. on p. 1).

[5] David J. Perreault, Khurram K. Afridi, and Iftikhar A. Khan. «32 - Automotive Applications of Power Electronics». In: *Power Electronics Handbook (Fourth Edition)*. Ed. by Muhammad H. Rashid. Fourth Edition. Butterworth-Heinemann, 2018, pp. 1067–1090. ISBN: 978-0-12-811407-0 (cit. on p. 1).

[6] *infineon.com*. https://www.infineon.com/dgdl/Infineon-Thermal_Modeling_of_Power_Electronic_Systems_3.0.pdf-ApplicationNotes-v01_00-EN.pdf?fileId=8ac78c8c92416ca501926358d80e4c65. [Accessed 27-01-2025] (cit. on p. 1).

[7] John Mathew and Shankar Krishnan. «A Review on Transient Thermal Management of Electronic Devices». In: *Journal of Electronic Packaging* 144.1 (Aug. 2021), p. 010801. ISSN: 1043-7398 (cit. on p. 1).

[8] Theodore L Bergman. *Fundamentals of heat and mass transfer*. John Wiley & Sons, 2011 (cit. on pp. 3, 4, 7, 10).

[9] Jingnan Li and Li Yang. «Recent Development of Heat Sink and Related Design Methods». In: *Energies* 16.20 (2023). ISSN: 1996-1073. URL: https://www.mdpi.com/1996-1073/16/20/7133 (cit. on p. 5).

[10] Xiaoxiao Guo, Shujian Cheng, Weiwei Cai, Yufeng Zhang, and Xue-ao Zhang. «A review of carbon-based thermal interface materials: Mechanism, thermal measurements and thermal properties». In: *Materials & Design* 209 (2021), p. 109936. ISSN: 0264-1275 (cit. on p. 5).

[11] *Physics:Thermal interface material - HandWiki — handwiki.org*. `https://handwiki.org/wiki/Physics:Thermal_interface_material`. [Accessed 26-04-2025] (cit. on p. 5).

[12] *Magnetic Cooling — refindustry.com*. `https://refindustry.com/articles/articles/magnetic-cooling/`. [Accessed 26-04-2025] (cit. on p. 6).

[13] Diana Enescu and Elena Otilia Virjoghe. «A review on thermoelectric cooling parameters and performance». In: *Renewable and Sustainable Energy Reviews* 38 (2014), pp. 903–916. ISSN: 1364-0321 (cit. on pp. 6, 7).

[14] *peltiermodules.com*. `https://peltiermodules.com/peltier.datasheet/TEC1-12706.pdf`. [Accessed 26-04-2025] (cit. on p. 6).

[15] Gareth Gilson, Stephen Pickering, David Hann, and Chris Gerada. «Piezoelectric Fan Cooling: A Novel High Reliability Electric Machine Thermal Management Solution». In: *Industrial Electronics, IEEE Transactions on* 60 (Nov. 2013), pp. 4841–4851. DOI: `10.1109/TIE.2012.2224081` (cit. on p. 8).

[16] X.L. Zhong, K.C. Chan, S.C. Fu, L.Q. Wang, and Christopher Y.H. Chao. «Enhancement of piezoelectric fan cooling by geometrical arrangements». In: *International Journal of Heat and Mass Transfer* 199 (2022), p. 123479. ISSN: 0017-9310 (cit. on p. 8).

[17] Mangesh Chaudhari, Bhalchandra Puranik, and Amit Agrawal. «Heat transfer characteristics of synthetic jet impingement cooling». In: *International Journal of Heat and Mass Transfer* 53 (Feb. 2010), pp. 1057–1069. DOI: `10.1016/j.ijheatmasstransfer.2009.11.005` (cit. on p. 8).

[18] Paweł Gil. «Flow and heat transfer characteristics of single and multiple synthetic jets impingement cooling». In: *International Journal of Heat and Mass Transfer* 201 (2023), p. 123590. ISSN: 0017-9310 (cit. on p. 8).

[19] Emmanouil D. Fylladitakis, Michael P. Theodoridis, and Antonios X. Moronis. «Review on the History, Research, and Applications of Electrohydrodynamics». In: *IEEE Transactions on Plasma Science* 42.2 (2014), pp. 358–375. DOI: `10.1109/TPS.2013.2297173` (cit. on p. 9).

[20] Andojo Ongkodjojo Ong, Alexis R. Abramson, and Norman C. Tien. «Electrohydrodynamic Microfabricated Ionic Wind Pumps for Thermal Management Applications». In: *Journal of Heat Transfer* 136.6 (Mar. 2014), p. 061703. ISSN: 0022-1481. DOI: 10.1115/1.4026807. eprint: https://asmedigitalcollection.asme.org/heattransfer/article-pdf/136/6/061703/6207074/ht_136_06_061703.pdf. URL: https://doi.org/10.1115/1.4026807 (cit. on p. 9).

[21] *grimsby.ac.uk*. https://www.grimsby.ac.uk/documents/defra/tech-thermoacoustic.pdf. [Accessed 02-05-2025] (cit. on p. 9).

[22] Seaho Song. «Thermal Performance Modeling and Measurements of Localized Water Cooled Cold Plate». In: Sept. 1993 (cit. on p. 10).

[23] Zhijun Wu, Guanyu Zhang, Shaoan Lu, Pengfei Leng, Yang Yu, Jun Deng, and Weidi Huang. «A comprehensive review of cold plate liquid cooling technology for data centers». In: *Chemical Engineering Science* 310 (2025), p. 121525. ISSN: 0009-2509 (cit. on p. 10).

[24] Ange-Christian Iradukunda, David R. Huitink, and Fang Luo. «A Review of Advanced Thermal Management Solutions and the Implications for Integration in High-Voltage Packages». In: *IEEE Journal of Emerging and Selected Topics in Power Electronics* 8.1 (2020), pp. 256–271. DOI: 10.1109/JESTPE.2019.2953102 (cit. on pp. 11, 12, 16).

[25] Jiangtao Cheng and Chung-lung Chen. «Adaptive Chip Cooling Using Electrowetting on Coplanar Control Electrodes». In: *Nanoscale and Microscale Thermophysical Engineering - NANOSCALE MICROSCALE THERMO E* 14 (Apr. 2010), pp. 63–74. DOI: 10.1080/15567261003601771 (cit. on p. 12).

[26] Niru Kumari and Suresh V. Garimella. «Characterization of the heat transfer accompanying electrowetting or gravity-induced droplet motion». In: *International Journal of Heat and Mass Transfer* 54.17 (2011), pp. 4037–4050. ISSN: 0017-9310 (cit. on p. 12).

[27] Eduardo Laloya, Óscar Lucía, Hector Sarnago, and José M. Burdío. «Heat Management in Power Converters: From State of the Art to Future Ultrahigh Efficiency Systems». In: *IEEE Transactions on Power Electronics* 31.11 (2016), pp. 7896–7908. DOI: 10.1109/TPEL.2015.2513433 (cit. on p. 13).

[28] Nugroho Agung Pambudi, Alfan Sarifudin, Ridho Alfan Firdaus, Desita Kamila Ulfa, Indra Mamad Gandidi, and Rahmat Romadhon. «The immersion cooling technology: Current and future development in energy saving». In: *Alexandria Engineering Journal* 61.12 (2022), pp. 9509–9527. ISSN: 1110-0168 (cit. on p. 13).

[29] Sreya Sarkar, Rohit Gupta, Tamal Roy, Ranjan Ganguly, and Constantine M. Megaridis. «Review of jet impingement cooling of electronic devices: Emerging role of surface engineering». In: *International Journal of Heat and Mass Transfer* 206 (2023), p. 123888. ISSN: 0017-9310 (cit. on p. 14).

[30] Govindarajan Natarajan and R. J. Bezama. «Microjet Cooler with Distributed Returns». In: *Heat Transfer Engineering* 28.8-9 (2007), pp. 779–787 (cit. on p. 14).

[31] S.M. Sohel Murshed and C.A. Nieto de Castro. «A critical review of traditional and emerging techniques and fluids for electronics cooling». In: *Renewable and Sustainable Energy Reviews* 78 (2017), pp. 821–833. ISSN: 1364-0321 (cit. on pp. 15, 16).

[32] Jobin Jose and Tapano Kumar Hotta. «A comprehensive review of heat pipe: Its types, incorporation techniques, methods of analysis and applications». In: *Thermal Science and Engineering Progress* 42 (2023), p. 101860. ISSN: 2451-9049 (cit. on p. 15).

[33] Jaeseon Lee and Issam Mudawar. «Two-phase flow in high-heat-flux micro-channel heat sink for refrigeration cooling applications: Part II—heat transfer characteristics». In: *International Journal of Heat and Mass Transfer* 48.5 (2005), pp. 941–955. ISSN: 0017-9310 (cit. on p. 16).

[34] Xiaochuan LIU, Guiping LIN, and Jinghui GUO. «Experimental study on the heat transfer performance of the two-phase spray cooling of Liquefied natural gas». In: *International Journal of Heat and Mass Transfer* 244 (2025), p. 126954. ISSN: 0017-9310 (cit. on p. 17).

[35] MR Pais, LC Chow, and ET Mahefkey. «Surface roughness and its effects on the heat transfer mechanism in spray cooling». In: (1992) (cit. on p. 17).

[36] Huseyin Bostanci, Daniel P. Rini, John P. Kizito, Virendra Singh, Sudipta Seal, and Louis C. Chow. «High heat flux spray cooling with ammonia: Investigation of enhanced surfaces for HTC». In: *International Journal of Heat and Mass Transfer* 75 (2014), pp. 718–725. ISSN: 0017-9310 (cit. on p. 17).

[37] Patrick Birbarah, Tarek Gebrael, Thomas Foulkes, Andrew Stillwell, Alexandra Moore, Robert Pilawa-Podgurski, and Nenad Miljkovic. «Water immersion cooling of high power density electronics». In: *International Journal of Heat and Mass Transfer* 147 (2020), p. 118918. ISSN: 0017-9310 (cit. on p. 17).

[38] Risako Kibushi, Kazuhisa Yuki, Noriyuki Unno, Tetsuro Ogushi, Masaaki Murakami, Tomiyuki Numata, Takuya Ide, and Hikaru Nomura. «Enhancement of the critical heat flux of saturated pool boiling by the breathing phenomenon induced by lotus copper in combination with a grooved heat transfer surface». In: *International Journal of Heat and Mass Transfer* 179 (2021), p. 121663. ISSN: 0017-9310 (cit. on pp. 17, 18).

[39] Ding Zhang, Heting Wu, Chris Bowen, and Ya Yang. «Recent Advances in Pyroelectric Materials and Applications». In: *Small* 17 (Oct. 2021) (cit. on pp. 21, 23, 63).

[40] Bingbin Wu, Habilou Ouro-Koura, Shao-Hao Lu, Huidong Li, Xueju Wang, Jie Xiao, and Zhiqun Daniel Deng. «Functional materials for powering and implementing next-generation miniature sensors». In: *Materials Today* 69 (2023), pp. 333–354. ISSN: 1369-7021 (cit. on p. 21).

[41] *TYDEX Lithium Niobate — tydexoptics.com*. `https://www.tydexoptics.com/materials1/materials_for_nonlinear_optics/lithium_niobate/`. [Accessed 18-06-2025] (cit. on p. 25).

[42] Volodymyr Tkachenko et al. «High-Rate Accumulation of Tiny Aqueous Droplets Using a Pyroelectrohydrodynamic Jet System». In: *Advanced Engineering Materials* 24.3 (2022), p. 2100756. eprint: `https://advanced.onlinelibrary.wiley.com/doi/pdf/10.1002/adem.202100756` (cit. on pp. 26, 27).

[43] Luigi Battista, Laura Mecozzi, Sara Coppola, Veronica Vespini, Simonetta Grilli, and Pietro Ferraro. «Graphene and carbon black nano-composite polymer absorbers for a pyro-electric solar energy harvesting device based on LiNbO3 crystals». In: *Applied Energy* 136 (2014), pp. 357–362. ISSN: 0306-2619 (cit. on pp. 26, 27).

[44] Eliodoro Chiavazzo, Luigi Ventola, Flaviana Calignano, Diego Manfredi, and Pietro Asinari. «A sensor for direct measurement of small convective heat fluxes: Validation and application to micro-structured surfaces». In: *Experimental Thermal and Fluid Science* 55 (2014), pp. 42–53. ISSN: 0894-1777 (cit. on p. 28).

[45] Nhlakanipho Mkhize and Harish Bhaskaran. «Electrohydrodynamic Jet Printing: Introductory Concepts and Considerations». In: *Small Science* 2.2 (2022), p. 2100073. eprint: `https://onlinelibrary.wiley.com/doi/pdf/10.1002/smsc.202100073` (cit. on p. 35).

[46] `http://wpage.unina.it/antcaval/lezioni/lez16.pdf`. [Accessed 05-07-2025] (cit. on p. 65).

[47] Nasser Ashgriz. *Handbook of Atomization and Sprays: Theory and Applications*. Jan. 2011. ISBN: 978-1-4419-7263-7. DOI: 10.1007/978-1-4419-7264-4 (cit. on p. 65).

Acknowledgements

I want to spend a few words to thank Professor Chiavazzo and Professor Bergamasco, who followed me through this thesis work. Thank you for your patience, and all the tips and help you gave me.

I also want to thank all the people who lent me a hand at CNR Isasi of Pozzuoli; in particular, a special thanks goes to researcher Sara Coppola, Zhe Wang and Professor Pietro Ferraro, who spent their precious time to help me accomplish this thesis results.

Thank you

Dedication

Dedico infine questa breve sezione della tesi per ringraziare tutte le persone che mi hanno permesso, tramite il loro supporto, di portare avanti questo progetto di laurea magistrale senza intoppi e con grande serenità.

In primis il mio più grande pensiero è rivolto ai miei genitori, mia madre Grazia e mio padre Massimo, senza i quali non sarei la persona che sono oggi. Li ringrazio per come mi hanno cresciuto ed educato, garantendomi sempre il supporto per fare qualunque cosa senza mai chiedere nulla in cambio. Grazie per avermi insegnato come stare al mondo e i valori che sono fiero di possedere, sono grato di avervi come genitori.

Ringrazio anche i miei nonni e le nonne che sono e sono stati. Ognuno di voi, a modo suo, ha saputo darmi serenità nella vita donandomi l'amore incondizionato di cui ognuno avrebbe bisogno.

Un grazie sincero va alla mia fidanzata Melania che mi sostiene da quando ho cominciato questo percorso di laurea magistrale. Grazie per mettermi sempre al primo posto, e grazie per tutte le belle parole che spendi per farmi sentire bene anche quando non le merito, ti amo.

Ringrazio tutte le persone che posso definire amici; in particolare i miei amici dalla scuola Pietro, Simone e Matteo, i miei ex colleghi Claudio, Orazio e Riccardo, quelli fatti nella strada Andrea e Matteo e chi conosco da una vita Daniele. L'amicizia non è qualcosa di scontato e mi ritengo fortunato ad avere persone che mi permettono di essere me stesso senza dovermi limitare. Grazie, questo risultato è stato raggiunto anche grazie a voi, spero non ci perderemo nelle molteplici strade che prenderanno le nostre vite.

Infine ringrazio anche tutti i miei cugini e cugine che pur essendo figlio unico si sono sempre comportati come fratelli e sorelle non facendomi sentire mai solo. Spero sinceramente che questo affetto rimanga immutato nel tempo.

Un grazie va anche a tutte le rimanenti persone che in qualche modo, anche in piccola parte, hanno reso possibile questo traguardo.

Grazie.